A new genus and species of frog from the Kem Kem (Morocco), the second neobatrachian from Cretaceous Africa

Alfred Lemierre [Corresp., 1], **David C. Blackburn** [2]

[1] Départmenet Origine et Evolution, UMR 7207, Centre de recherche en Paléontologie, CNR/Sorbonne Université/MNHN, Museum national d'Histoire naturelle, Paris, France

[2] Department of Natural History, Florida Museum of Natural History, University of Florida, Gainesville, Florida, United States

Corresponding Author: Alfred Lemierre
Email address: alfred.lemierre@edu.mnhn.fr

Neobatrachia, a clade representing the majority of extant anuran diversity, is thought to have emerged and diversified during the Cretaceous. Most of early diversification of neobatrachians occurred in southern Gondwana, especially the regions that are today South America and Africa. Whereas five extinct neobatrachians have been described from the Cretaceous of South America in the last decade, only one is known from Africa. This difference in the known extinct diversity is linked to the lack of well-preserved specimens, understudy of fragmentary remains, and lack of known Cretaceous sites in Africa. Study of fragmentary anurans remains from Africa could allow for the identification of previously unknown neobatrachians, allowing for a better understanding of their early diversification. We reanalysed several previously described anuran specimens from the well-known Kem Kem beds, including using CT-scanning. Through our osteological study, we determined that several cranial bones and vertebrae represent a new hyperossified taxon, *Cretadhefdaa taouzensis*. Comparison to other hyperossified anurans revealed similarities and affinity with the neobatrachians *Beelzebufo* (extinct) and *Ceratophrys* (extant). Phylogenetic analyses supported this affinity, placing *Cretadhefdaa* within Neobatrachia in an unresolved clade of Ceratophryoidea. *Cretadhefdaa* is the oldest neobatrachian from Africa, and reveals that neobatrachians were already widespread throughout southern Gondwana during the earliest Late Cretaceous.

A new genus and species of frog from the Kem Kem (Morocco), the second neobatrachian from Cretaceous Africa

Alfred Lemierre[1], David C. Blackburn[2]

[1.] CR2P- Centre de recherche en Paléontologie-CNRS/MNHN/Sorbonne Université, Paris, 75005, France

[2.] Department of Natural History, Florida Museum of Natural History, University of Florida, Gainesville, FL 32611, USA

Corresponding Author:

Alfred Lemierre[1]

Email address: alfred.lemierre@edu.mnhn.fr

Abstract

Neobatrachia, a clade representing the majority of extant anuran diversity, is thought to have emerged and diversified during the Cretaceous. Most of early diversification of neobatrachians occurred in southern Gondwana, especially the regions that are today South America and Africa. Whereas five extinct neobatrachians have been described from the Cretaceous of South America in the last decade, only one is known from Africa. This difference in the known extinct diversity is linked to the lack of well-preserved specimens, understudy of fragmentary remains, and lack of known Cretaceous sites in Africa. Study of fragmentary anurans remains from Africa could allow for the identification of previously unknown neobatrachians, allowing for a better understanding of their early diversification. We reanalysed several previously described anuran specimens from the well-known Kem Kem beds, including using CT-scanning. Through our osteological study, we determined that several cranial bones and vertebrae represent a new hyperossified taxon, *Cretadhefdaa taouzensis*. Comparison to other hyperossified anurans revealed similarities and affinity with the neobatrachians *Beelzebufo* (extinct) and *Ceratophrys* (extant). Phylogenetic analyses supported this affinity, placing *Cretadhefdaa* within Neobatrachia in an unresolved clade of Ceratophryoidea. *Cretadhefdaa* is the oldest neobatrachian from Africa, and reveals that neobatrachians were already widespread throughout southern Gondwana during the earliest Late Cretaceous.

39

40

41

42 Introduction

43 The Cretaceous is a key period in anuran evolution and diversification including the emergence
44 of major extant clades such as the Neobatrachia and Pipidae (Frazão et al., 2015; Feng et al.,
45 2017). The breakup of the Western Gondwana palaeocontinent during the Late Jurassic and
46 Early Cretaceous (McLoughlin, 2001; Blakey et al., 2008)—leading to the creation of the Central
47 and Southern Atlantic Oceans—may have contributed to the early diversification of the
48 Neobatrachia, just as it likely did for the Pipidae (Frazão et al., 2015; Feng et al., 2017). Several
49 neobatrachian taxa have been described in the last decade from the Cretaceous beds of South
50 America (Báez et al., 2009; 2012; Báez and Gómez, 2018; Agnolin et al., 2020), contributing to a
51 better understanding of early diversification of the Neobatrachia. Unfortunately, the fossil
52 record of Neobatrachia is scarce for the Cretaceous of Africa and includes only a single
53 described taxon: *Beelzebufo ampinga* from the Cretaceous of Madagascar (Evans et al., 2014).
54 However, the lack of both study and sampling is not limited to either African Cretaceous
55 outgroups or extinct Neobatrachia. In general, there are few well-preserved and identifiable
56 anuran fossils in Africa, with numerous sites yielding only few and fragmentary remains (e.g., de
57 Broin et al., 1974; Báez and Werner, 1996; Rage, 2008; Gardner and Rage, 2016) that are not
58 easily incorporated into phylogenetic analyses. This contrasts with South American

neobatrachians, several of which are known from well-preserved and mostly articulated specimens preserving much or all of the skeleton (Báez et al., 2012). In Africa, only a handful of sites contain enough fragmentary fossils referred to the same taxon to allow for comparisons to other frogs and inclusion in phylogenetic analyses (Evans et al., 2008, 2014). These few sites are critical to filling the gap in the fossil record of Neobatrachia and central to understanding their early diversification in Africa.

The Kem Kem beds of Morocco (Cretaceous, 100 95 Ma; Ibrahim et al., 2020) are known for their rich terrestrial vertebrate fauna with numerous dinosaurs, fishes, sharks, turtles, and crocodiles (Zouhri, 2017). This fauna has been studied extensively in recent decades (Ibrahim et al., 2020) but there is only a single study of its amphibians. Rage and Dutheil (2008) provided evidence for three different anurans, including one pipid that they described as *Oumtkoutia anae* based on a neurocranium, as well as two indeterminate non-pipid anurans based on postcranial remains (Rage and Dutheil, 2008). They attributed several cranial fragments to an undescribed species (mainly based on relative size of the cranial and postcranial elements) with an ornamented and hyperossified skull, one of the earliest known from the Cretaceous of Africa. Agnolin (2012) later described a neobatrachian taxon (Calyptocephalellidae) from the Late Cretaceous of Argentina and reviewed several Gondwanan anurans with hyperossified skulls. In that study, he included the Kem Kem fossils which he referred to the Calyptocephalellidae based on cranial and postcranial characters. Because several subsequent studies (Báez and Gómez, 2018; Muzzopappa et al., 2020) highlighted anatomical and analytical errors in Agnolin (2012), the attribution of the Kem Kem fossils to the Calyptocephallelidae is questionable. Because Agnolin (2012) considered all of the “indeterminate” anuran remains

from the Kem Kem to be a single taxon in his study, several characters supporting the affiliation these fossils with the Neobatrachia are based on postcranial elements not clearly referable to the hyperossified cranial elements. Further, because Agnolin (2012) did not included the Kem Kem fossils in his phylogenetic analysis, their relationships were never formally tested. Revaluation of the anatomy and phylogenetic affinities of this hyperossified Kem Kem frog may be important for deciphering the early diversification of neobatrachians during the Lower Late Cretaceous of Gondwana and filling a notable gap in the fossil record of African anurans.

Here, we use microcomputed tomographic scans (MicroCT scans) to provide new information about the anatomy of the hyperossified Kem Kem frog. These new data allow for a more complete anatomical study of this taxon, comparisons to other Cretaceous anurans, and a phylogenetic analysis to estimate its relationships. We describe this material as a new genus and discuss its importance for understanding neobatrachian diversification in Gondwana during the Cretaceous.

Geological Context

The specimens were collected in 1995 during an expedition organized by the University of Chicago and the Service géologique du Maroc at four different localities near Taouz and Oum Tkout (OT1c, TD1, TZ8a1 and TZ8a2 from Dutheil, 1999) from the Kem Kem beds (Ettachfini and Andreu, 2004; Cavin et al., 2010). The term “Kem Kem beds” (Sereno et al., 1996) refers to a large escarpment extending across southeastern Morocco, near the Morocco-Algerian border (Ibrahim et al., 2020: fig. 1A, C), with numerous exposures along its length. More recently,

these beds have been referred to as the Kem Kem group (Ibrahim et al., 2020), containing two formations: the Gara Sbaa and the Douira Formations. The anuran specimens discussed here were recovered from layers that can be correlated to the Douira Formation of the Kem Kem group (upper part of the Kem Kem; Ibrahim et al., 2020). The Douira Formation (as well as the Gara Sbaa Formation) has been correlated to the Bahariya Formation in Egypt (Sereno et al, 1996; Cavin et al., 2010), which is dated to the Early Cenomanian (Cavin et al., 2010). The Kem Kem group is topped by marine sediments correlated to the Cenomanian-Turonian transition (Cavin et al., 2010). Other analyses have confirmed the Cenomanian age (Ibrahim et al., 2020) and considered the Kem Kem group a single continuous deposit sequence from 100 to 95 Ma. The boundary between the Gara Sbaa and the Douira Formations is dated to 96 Ma and linked to the Mid-Cenomanian Event (Ibrahim et al., 2020). The Douira Formation—and the anuran specimens discussed here—are thus dated from the middle Cenomanian, approximately 96 to 95 Ma (Ibrahim et al., 2020).

The Douira Formation contains strata that show a marine influence that increases over time. The deposits in the lower part of the formation, composed of sandstones and mudstones, are consistent with a river delta, whereas the deposits in the upper part, composed of interbedded mudstone with claystone, are characteristic of coastal and sabkha environments (see Ibrahim et al., 2020 for a complete description). There is no indication if the materials came from either lower or upper part of the Douria Formation.

Materials and Methods

Institutional Abbreviations

MNHN: Muséum National d'Histoire Naturelle, Paris (France); **UCRC-PV**: University of Chicago research collection, Chicago (USA)

The anuran fossils are curated in the vertebrate palaeontology research collection of the University of Chicago. We generated MicroCT scans at the University of Florida's Nanoscale Research Facility using a Phoenix v|tome|x M (GE Measurement & Control Solutions, Boston, MA, USA). Voltage and current were customized for each specimen to balance resolution and intensity contrast; scanning parameters are included in the metadata associated with the scans on MorphoSource. The x-ray images were converted into tomogram slices using GE's reconstruction software datos|x (see Table S1 in Supplemental Data 1). Each stack of slices produced was imported in the 3D reconstruction software Mimics 21.0 (Materialise, Leuven, Belgium); before importation, slices were cropped to remove empty spaces. To further decrease the data size, the slices were converted from 16 bits to 8 bits. The resulting slices have an image resolution of 1580 × 2144 pixels and a voxel size of 5.7 µm for the volume size. 3D models were produced by segmenting each element using the 'thresholding' function (using the contrast on greyscale images). 3D model of the endocast was produced by segmenting each element using the "add" function. We used the same voxel resolution of 5.7 µm, with a smoothing factor of 3 for one iteration, to homogenize the model resulting from the segmentation. Data produced by segmentation were exported in the software 3matic 9.0 as separate files (see Table S1 in Supplemental Data 1).

143 The electronic version of this article in Portable Document Format (PDF) will represent a
144 published work according to the International Commission on Zoological Nomenclature (ICZN),
145 and hence the new names contained in the electronic version are effectively published under
146 that Code from the electronic edition alone. This published work and the nomenclatural acts it
147 contains have been registered in ZooBank, the online registration system for the ICZN. The
148 ZooBank LSIDs (Life Science Identifiers) can be resolved and the associated information viewed
149 through any standard web browser by appending the LSID to the prefix http://zoobank.org/.
150 The LSID for this publication is: urn:lsid:zoobank.org:pub:DCACD333-53AA-4A6D-A0F0-
151 9F9C180F0DD. The online version of this work is archived and available from the following
152 digital repositories: PeerJ, PubMed Central SCIE and CLOCKSS.

153 **Phylogenetic analyses**

154 Our data matrix includes 88 taxa and 150 morphological characters (62 cranial and 75
155 postcranial characters, 12 from the hyobranchial apparatus, and one from soft-tissues) and is
156 derived from that of Lemierre et al. (2021; see Appendix S1 3). We added two extinct
157 hyperossified neobatrachian taxa (the new taxon described below from the Kem Kem, and
158 *Hungarobatrachus szukacsi*) to test their affinities. *Hungarobatrachus szukacsi* Szentesi and
159 Venczel, 2010 has recently been included into a reduced phylogenetical analysis (ref Venczel et
160 al, 2021), and considered a neobatrachian. It is the oldest neobatrachian outside of Gondwana
161 and essential to understand the diversification of the clade during the Cretaceous. These new
162 taxa were scored from observation on 3D mesh files created for this study based on segmenting
163 newly generated MicroCT scans (see above) and from literature (Szentesi and Venczel, 2010;
164 Venczel et al., 2021).

All analyses were performed using TNT v.1.5 (Goloboff and Catalano, 2016). All analyses were conducted with cline (also called multi-state) characters ordered (characters 3, 9, 10, 14, 26, 34, 51, 52, 68, 93, 112, 121, 124, 125 and 126). Cline characters were ordered as several studies (Rineau et al., 2015, 2018) showed that analyses using ordered morphocline characters outperformed analyses using unordered characters, even when the ordering scheme is wrong (Rineau et al., 2018). Analyses consisted of heuristic searches with 1000 random addition sequences of taxa, followed by tree bisection reconnection (TBR) branch swapping, withholding 10 trees per repetition. The final trees were rooted using *Ascaphus truei* (Ascaphidae, Anura) and a strict consensus was created. Node supports were evaluated using Bremer support and standard nonparametric bootstrapping, with searches of 1000 replicates and collapsing groups below 5% frequency.

Because the phylogeny resulting from above is strongly at odds with relationships inferred from those inferred with molecular genetic data, we performed an additional analysis using a constraint tree reflecting a consensus of recent molecular phylogenetic analyses. This included constraining the backbone of the tree to reflect early divergences in anuran evolution, as well as large-scale patterns of relationships within the two major clades of Neobatrachia (Hyloidea, Ranoidea). We did not constrain the placement of any extinct taxa and we also left relationships within major clades as polytomies so that relationships within them could be inferred by our morphological dataset. We based this constraint tree (available in the Supplemental Materials) primarily on recent phylogenomic analyses, including Feng et al (2017), Streicher et al. (2018), Yuan et al. (2018), and Hime et al. (2021).

Results

Systematic Paleontology

ANURA Duméril, 1804

NEOBATRACHIA Reig, 1958

CRETADHEFDAA gen. nov.

Type (and only known) species

Cretadhefdaa taouzensis sp. nov.

CRETADHEFDAA TAOUZENSIS sp. nov.

Holotype

UCRC-PV94, posterior braincase preserving incomplete frontoparietals, parasphenoid, and prooticooccipitals.

Type locality

TD1, near the city of Taouz in southeastern Morocco (see Dutheil, 1999 for more information on Kem Kem localities).

Stratigraphic range

Middle Cenomanian (96–95 Ma).

Referred materials

One incomplete squamosal from TD1 (UCRC-PV95); one incomplete maxilla from Tz8a1 (UCRC-PV96); three incomplete presacral vertebrae, two from TD1 (UCRC-PV97–98) and one from Tz8a1 (UCRC-PV101); one incomplete sacral vertebra from OT1c (UCRC-PV103).

Etymology

The genus nomen *Cretadhefdaa* is a combination of the word Cretaceous and a transliteration of the pronunciation of the Arabic word ضفدع or *dhefdaa* (also sometimes written as *dheftha* or *thedfaa*), meaning "frog." The specific epithet *taouzensis* recognizes the type locality, Taouz.

Diagnosis

A neobatrachian anuran with a hyperossified skull differing from all other anurans by the following unique combination of characters: frontoparietals coossified, lacking a midline suture, and covered in ornamentation of pits and ridges; frontoparietals bearing a smooth occipital flange; no incrassatio frontoparietalis on the ventral surface of the frontoparietals; presence of a deep, groove-like central recess on the posterodorsal surface of the braincase to each side of the foramen magnum, and housing the foramen for the occipital artery. Diagnosis for the species is same as for the genus.

Description of the holotype (UCRC-PV94)

Osteological description

UCRC-PV94 is the preserved posterior region of the braincase of *Cretadhefdaa*. All bones are co-ossified and the sutures between the prooticooccipitals and frontoparietals are difficult to discern (Fig. 1A–G).

The posterior portion of the frontoparietals is preserved. The two frontoparietals are coossified to one another, and no suture is visible on the frontoparietal table (Fig. 1A). The frontoparietal table is large and covered in an ornamentation of pits and ridges. The posterior margin of the frontoparietals is flanked by a large occipital flange that lacks ornamentation (Fig. 1A). The processes paraoccipitalis are reduced and fused to the underlying epiotic eminence (prominentia circularis ducti of Roček and Lamaud, 1995), and the posterior process is not distinct (Fig. 1A). There is no pineal foramen visible. In lateral view, the preserved portion of the pars contacta is a straight vertical lamina (Fig. 1B). Because the lateral expansion of the frontoparietal is broken along its entire length, its full extent is unknown. In ventral view, the frontoparietal table extends lateral to the pars contacta into a tectum supraorbitale, but its full extent is unknown because it is broken (Fig. 1A, B). There is no visible frontoparietal incrassation on the ventral surface of the frontoparietals. In posterior view, the boundary between the frontoparietals and prooticoccipital bears a series of deep recesses (Fig. 1D, E). The recesses are located between the tall epiotic eminence and the posterior margin of the frontoparietal table and appear to form a single large, deep groove on each side of the braincase. However, three different recesses can be distinguished within each groove (medial, central, and lateral recesses in Fig.1E) that are each separated by well-defined ridges. Both the lateral and medial recesses are shallow, whereas the central recess is deep and houses a large,

circular foramen for the occipital artery. The exit foramen for the occipital artery is visible on each lateral surface of the frontoparietal, ventral to the lateral extension of the table (Fig. 1B).

The posterior region of the parasphenoid is preserved. The cultriform process is broken, preserving only its base. The alae are large and cover the ventral surface of the otic capsules. In ventral view, the alae bear a median keel on its surface, extending from its lateral margin to and slightly curving towards the posterior process of the bone (Fig. 1C). The posterior process is divided into two well-separated small extensions, oriented posterolaterally. These expansions are fused to the base of the occipital condyles (Fig. 1C).

The prootic and exoccipital are coossified into a single prooticooccipital complex without a visible suture. Each prooticooccipital is co-ossified to the other along their medial margins, as well as to the frontoparietals (dorsally) and parasphenoid (ventrally). In dorsal view, the epiotic eminence is large, forming a broad lamina (Fig. 1A, D). The dorsal surface of the prootic is smooth. The crista parotica is not fully preserved, but likely extended laterally. There is no trace of an articulation facet with the squamosal on the preserved portion of the prooticoccipital (Fig. 1A). In anterolateral view, a large prootic foramen is present on the anterior surface of the prooticoccipital (Fig. 1B, F), and is fully enclosed in bone. In lateral view, anterior to the prootic foramen, a notch is visible on the anteriormost bony margin of the braincase (Fig. 1B) and might represent the posterior portion of the optic foramen. In anterior view, a well-delimited, narrow groove, likely for the jugular vein, extends from a large depression at the border of the prootic foramen to the lateral margin of the prootic (Fig. 1F). Beneath this groove, a large depression is present from the lateral margin of the prootic to the midpoint of its anterior surface. This is likely an articular facet for the medial ramus of the pterygoid. In posterior view,

the left occipital condyle is missing (Fig. 1D), but the right occipital condyle is slightly ventrolateral to the large foramen magnum (Fig. 1D). The occipital condyle obscures the jugular foramen that remains partially visible laterally (Fig. 1D). In medial view, several foramina are visible in the wall of the braincase. The posteriormost opening is the jugular foramen (Fig. 1G). Separated from the latter foramen by a thin bony pillar, a large opening is present on the lateral braincase wall (Fig. 1G). This opening likely represents the fused acoustics foramina. This fusion might be the result of damage during the preservation, or by the absence of a bony separation between the two foramina. A similar preservation is also present in the exceptionally preserved *Thaumastosaurus servatus* Filhol 1877 (Lemierre et al., 2021).

Inner Ear

The preservation of the otic capsule allowed us to segment the otic chamber and semi-circular canals (vestibular apparatus) of *Cretadhefdaa*. The anterior, posterior, and lateral canals are all preserved and clearly identifiable (Fig. 2A, B). In anterior view, the base of the anterior canal bears a bulge, containing the anterior ampulla (Fig. 2A). In dorsal view, at the base of both anterior and lateral canals, the bulges contain the anterior and lateral ampullae (Fig. 2C). At the base of the posterior sinus (connecting the lateral and posterior canals), a similar bulge contains the posterior ampulla (Fig. 2B, D). In anterior and posterior views, the superior sinus (common crus), connecting the anterior and posterior canals, is well preserved (Fig. 2A C). The base of the superior sinus is thick, and is part of the utricle. The utricle forms the ventral portion of the vestibular apparatus. The vestibular apparatus occupies approximately half of total height of the endocast. The auditory region is large and bulbous (Fig. 2), and the perilymphatic cistern occupies most of the endocast. Lateral to the perilymphatic cistern, a small region is delimited

from the rest of the ventral volume by a slight constriction (Fig. 2A, B). This region can be identified as the lateral chamber (Wever, 1979). The posterolateral surface of the lateral chamber bears a flattened surface, that corresponds to the oval window, where the footplate of the columella (and the operculum if present) would have abutted the inner ear (Wever, 1985; Maddin et al., 2013). In the posteromedial region of the perilymphatic cistern, a short and large canal, representing the perilymphatic duct, opens posteriorly (Fig. 2B, D) into the braincase and the condyloid fossa (i.e., “round window”; Wever, 1985). Another large duct is visible in the medial region of the otic chamber, entering the braincase through the fused acoustic foramina. However, this canal comprises two smaller ducts that are fused medially (Fig. 2) and housed the pathway of the cranial nerve VIII (Gaupp, 1896), representing the acoustic nerve (Duellman and Trueb, 1994). This confirms that the large foramina of the medial wall of the braincase is the fusion of the two acoustic foramina of *Cretadhefdaa*. A second medial, smaller duct is visible in the medial region of the vestibular apparatus, leading to the dorsalmost foramen of the medial wall of the braincase (Fig 1G). This duct is identified as the endolymphatic duct, leading to the endolymphatic sac that was present in the braincase (Frishkof and Goldstein, 1963; Duellman and Trueb, 1994).

Referred Cranial Material

UCRC-PV95

The specimen is a fragment of a right squamosal preserving a part of the otic plate (ramus paroticus) and the posterior process. The dorsal and lateral surface of the bone is covered with an ornamentation made of deep longitudinal pits and ridges in the anterior and temporal

region, and deep, nearly circular pits and ridges in the posterior and otic region. This ornamentation is slightly different from that observed in UCRC-PV94, though it is not uncommon for anuran cranial bones to display variation in ornamentation within an individual (Buffrénil et al., 2015, 2016). Thus, we interpret UCRC-PV95 as belonging to the same taxon as UCRC-PV94. The size of the squamosal is consistent with the size of the braincase (UCRC-PV94), but there is no indication that the two bones belong to the same individual. The otic plate is well developed (~3 mm length, anterior to posterior) and bears a vertical lamina on its ventral surface near the medial margin of the plate. On this lamina, a small ventral ridge is present, and delimits several ventral recesses. This system of ventral ridge and recesses resembles the one recovered in *Beelzebufo ampinga* (Fig. 3; Evans et al., 2014: fig. 18). In *Beelzebufo*, this system has been interpreted as an interlocking joint for the lateral end of the crista parotica (Evans et al., 2014). A similar interpretation can be made for *Cretadhefdaa*. This indicates that the squamosal extended medially and contacted the frontoparietals. However, we cannot be certain whether the squamosal covered the entire dorsal surface of the otic capsule (as in *Beelzebufo*) or if a supratemporal fenestra was present.

The posterior process is thick and elongate mediolaterally. Its medial surface is concave towards its center and forms a shallow recess near the junction of the posterior process and the otic plate. The posterior margin lacks ornamentation and bears a shallow depression on its ventral surface. The ventral margin of the posterior process is straight. The shallow depression was likely an articular facet for the quadratojugal (Fig. 3).

UCRC-PV96

This represents the middle portion of a left maxilla. The maxilla is toothed and its lateral surface is covered in a pits and ridges ornamentation. The ornamentation covers almost all of the lateral surface, save for a thin strip of bone ventrally and its dorsalmost portion. Dorsally, the base of a large process is preserved. It likely served as an articular facet with the squamosal. In medial view, the pars dentalis is straight, with a small sulcus dentalis (visible in ventral view). The lamina horizontalis is faint, almost non-distinct from the medial surface of the maxilla. It forms a small ridge, with a shallow dorsal groove for the palatoquadrate. A deep maxillary recess is present medially. A groove for maxillary nerves extends dorsally from the maxillary recess to the dorsal part of the maxilla. This groove delimits a small articular facet oriented dorsomedially. It could be a facet for articulation with the palatine (neopalatine of Trueb, 1973). Because only the bases of several teeth are preserved, nothing can be said of the tooth morphology of *Cretadhefdaa*.

Referred Vertebrae

The four vertebrae attributed to *Cretadhefdaa* all have an anterior cotyle and a posterior condyle, indicating a procoelous condition of the vertebral column. Although the shape of the centrum varies among these specimens (UCRC-PV97, UCRC-PV101 and UCRC-PV103 are shorter than UCRC-PV98), their similar size and the shape of articular facets and zygapophyses suggests that they all represent the same taxon. In addition, the two best preserved vertebrae, UCRC-PV101 and UCRC-PV98, each has a similarly shaped low and short neural spine that is oriented posteriorly. In other anurans, there is documented variation in the length of the centra of

presacral vertebrae throughout the vertebral column (Evans et al., 2014; Lemierre et al., 2021: fig. 9). We attribute the above cranial elements and these vertebrae to *Cretadhefdaa* because they all represent non-pipid individuals of similar body size (following Rage and Dutheil, 2008).

UCRC-PV97

This specimen is a centrum of a procoelous vertebra, with the neural walls not preserved (Fig. 4A–C). The centrum is longer than wide (Fig. 4A, B). The posterior condyle is large and wide.

UCRC-PV98

This presacral vertebra is better preserved than UCRC-PV97, with most of the transverse process, one postzygapophysis, and the distal end of the neural spine missing (Fig. 4D–I). The width of the posterior condyle is the same as that of the vertebral canal. The neural walls are thick, with the base of the transverse processes protruding laterally. In dorsal view, the remnants of the transverse processes are subcylindrical and oriented posteriorly. Each prezygapophysis bears a large flat and ovoid-shaped articular facet that is oriented dorsomedially (Fig. 4F). The medial margin of this articular facet is a sharp, straight lamina constituting the medial end of the dorsal wall of the anterior vertebral canal. The neural spine is low and was likely short, though it is broken distally. The postzygapophysis is long, with an ovoid and flattened articular surface that is oriented ventrally (Fig. 4F). A small posterior lamina connects the neural spine and the medial margin of the postzygapophysis. The centrum is more elongate than UCRC-PV97 (Fig. 4G). In ventral view, the centrum is compressed lateromedially at midlength, giving the ventral surface an hourglass shape (Fig. 4G). In lateral view, a shallow depression with a blind foramen is visible at the midpoint of the vertebra and is likely a spinal

foramen (Fig. 4H, I). The elongate centrum indicates that this vertebra is from the mid-column of *Cretadhefdaa*, possibly representing presacral vertebra IV.

UCRC-PV101

This element is an incomplete presacral vertebra preserving the centrum and neural arch (Fig. 4J–N). The centrum is short, almost as wide as large. The vertebra is procoelous, with an anterior cotyle and a posterior condyle (Fig. 4J, K). The condyle is poorly preserved but seems elongate lateromedially. The prezygapophyses bear a flat articular facet that is oriented dorsomedially (Fig. 4L). In dorsal view, the anterior margin of the neural arch is concave posteriorly, and a sharp ridge is visible on the dorsal surface of the neural arch, marking the beginning of the neural spine. The neural spine is very short (shorter than the one recovered in UCRC-PV98) and oriented posteriorly. Each postzygapophysis bears a flat articular surface that is oriented ventrolaterally. The transverse processes are broken at their bases. The base of these processes is cylindrical in shape and elongate anteroposteriorly, oriented perpendicular to the anteroposterior axis of the centrum (Fig. 4L, N). The anteroposteriorly short centrum and the low and posteriorly oriented neural spine indicate that UCRC-PV101 is one of the posterior presacral vertebra (VI to VIII). The posterior condyle of UCRC-PV101 is similar in size to the anterior cotyle of the identified sacral vertebra (UCRC-PV103) and the inferred position of the prezygapophyses of UCRC-PV103 seems to match the position of the postzygapophyses of UCRC-PV101. UCRC-PV101 might represent the last presacral vertebra (VIII).

UCRC-PV103

This incomplete sacral vertebra bears an anterior cotyle and two posterior condyles (Fig. 4O–R). The centrum of UCRC-PV103 is shorter than the other three vertebrae, but the anterior cotyle is similar to those of UCRC-PV97–98 and 101. The two posterior condyles are well separated and are wider than tall, and thus elliptical. The preserved transverse process is posterolaterally oriented and the preserved portion does not expand distally. In lateral view, the sacral transverse process is extended anteroposteriorly, and is not cylindrical or rod-like. The dorsal expansion of the transverse process is visible in dorsal view (Fig. 4R).

Osteological comparison to hyperossified anurans

Hyperossified (sensu Trueb, 1973) ornamented cranial bones occur in both extinct and extant anurans, from pipoids (Báez and Rage, 1998; Trueb et al., 2000) to diverse lineages of neobatrachians, and has evolved more than 20 times independently across extant frogs (Paluh et al., 2020). Hyperossified cranial elements are known in numerous Cretaceous anurans from both Laurasian and Gondwanan sites (Jacobs et al., 1990; Rage and Roček, 2003; Roček, 2013; Gardner and Rage, 2016). In the Gondwanan fossil record, Cretaceous hyperossified anurans are known that belong to both the Pipimorpha and Neobatrachia (Gardner and Rage, 2016; Gómez and Báez, 2018).

Comparison to non-neobatrachian taxa

Ornamented and co-ossified cranial bones are relatively uncommon in the first four diverging lineages of extant frogs: Leiopelmatoidea, Alytoidea, Pipoidea, and Pelobatoidea. Neither of the two extant leiopelmatoids, *Ascaphus* and *Leiopelma*, exhibit any characteristics unique to hyperossified anuran skulls. Among the extant alytoids, ornamented dermal bones are found

413 only in the genus *Latonia* which is known from the Paleogene and Neogene of Laurasia and
414 Africa (Roček, 1994; 2013; Biton et al., 2016). However, *Cretadhefdaa* differs from *Latonia* in
415 having a foramen for the occipital artery (lacking in *Latonia*) and frontoparietals that coalesce
416 and fuse with the prooticooccipitals (see Roček, 1994: fig. 7). The extinct Gobiatidae from the
417 Cretaceous of Asia (Roček, 2008; 2013) also exhibits ornamented dermal bones. However,
418 *Cretadhefdaa* can be differentiated from all Gobiatidae in having fused frontoparietals without
419 a visible suture (frontoparietals not fused or in contact with each other in Gobiatidae),
420 complete fusion of the prootic and exoccipital (suture visible between the two bones in
421 Gobiatidae; Roček, 2008), and presacral vertebrae that are procoelous (amphicoelous in
422 Gobiatidae).

423 *Cretadhefdaa* can be differentiated from all pipoid anurans in having alae of the parasphenoid
424 that cover the ventral surface of the otic capsules (Fig. 1C). Some members of the Pelobatoidae
425 also have ornamented skull bones, but as an integral part of the bone and not as a secondary
426 exostosis (Rage and Roček, 2007; Roček, 2013; Roček et al., 2014) as seen in *Cretadhefdaa*. In
427 addition, several fragmentary remains of ornamented maxillae and procoelous vertebrae were
428 recovered in the Cretaceous outcrops of Texas and might represent one the early diverging frog
429 lineages, but the phylogenetic affinities of these fossils remain unclear (Roček, 2013). Based on
430 these comparisons, we exclude *Cretadhefdaa* from the Leiopelmatoidea, Alytoidea, Pipoidea,
431 and Pelobatoidea.

432 The vast majority of extant frog species belong to the Neobatrachia. *Cretadhefdaa* shares with
433 Neobatrachia the presence of well-separated occipital condyles and a bicondylar articulation
434 between the sacrum and urostyle. However, the principal synapomorphies used to diagnose

435 Neobatrachia, such as the presence of palatines (also called neopalatines in neobatrachians;
436 Báez et al., 2009) cannot be assessed based on the preserved elements of *Cretadhefdaa*.

437 **Comparison to Cretaceous hyperossified taxa**

438 The best known non-pipimorph ornamented taxon described from the Mesozoic fossil record of
439 Africa is *Beelzebufo ampinga* Evans et al. 2008¸ from the Maastrichtian of Madagascar (Evans et
440 al., 2008, 2014). *Beelzebufo* is known from numerous cranial and some postcranial elements.
441 The ornamentation of *Cretadhefdaa*, comprised of pits and ridges, is similar to that of
442 *Beelzebufo*. Both taxa also have a series of three recesses on the posterodorsal surface of the
443 braincase, with the foramen for the occipital arteria located within the central recess, which is
444 the deepest recess in both taxa (Fig. 5). *Cretadhefdaa* also differs from *Beelzebufo* in having a
445 smooth occipital flange on the posterior region of the frontoparietals. The poor preservation of
446 the lateral expansion of the frontoparietals of *Cretadhefdaa* (UCRC-PV94) means that we
447 cannot evaluate whether it is similar to the expansion in *Beelzebufo*, in which the lateral
448 expansion is elongate laterally along on its entire length, covering the lateral region of the
449 braincase (Evans et al., 2014). The parasphenoid of *Cretadhefdaa* is similar to that of *Beelzebufo*
450 in having narrow alae (alary process of Evans et al., 2014) with a median keel. *Cretadhefdaa* is
451 similar to *Beelzebufo* in lacking a distinct palatine shelf on the medial surface of the maxilla, but
452 differs in having ornamentation of the pars facialis on the lateral surface of the maxilla that
453 extends ventrally to the pars dentalis (the ornamentation ends before the pars dentalis in
454 *Beelzebufo*).

455 The presacral vertebrae of *Cretadhefdaa* differ from most of those referred to *Beelzebufo* by
456 lacking a well-developed neural spine that is both tall and thick as well as the expanded and
457 ornamented “table” sitting atop the spine (Evans et al., 2014: fig. 34–36); even the shortest
458 neural spine of the posteriormost presacral of *Beelzebufo* is taller than that of any vertebrae
459 that we refer to *Cretadhefdaa* (Fig. 4F, L). The sacral vertebra of *Cretadhefdaa* is similar to that
460 of *Beelzebufo* in having two elliptical posterior condyles for the sacro-urostylar articulation and
461 a centrum that is wider than longer (Fig. 4P). However, the sacral transverse processes of
462 *Beelzebufo* are slightly more expanded distally than that preserved for *Cretadhefdaa* (Fig. 4R).

463 Another neobatrachian from Gondwana with an ornamented skull is *Baurubatrachus pricei*
464 Báez and Perí, 1989 from the Crato Formation of Brazil (Upper Early Cretaceous). The poor
465 preservation of the frontoparietals of the holotype (and only known specimen), which is still
466 embedded in matrix, prevents comparisons of the braincase of *Cretadhefdaa* to
467 *Baurubatrachus*. However, its frontoparietals seem similar in having ornamentation comprised
468 of pits and ridges that extend posteriorly to the margin of the foramen magnum. *Cretadhefdaa*
469 also differs from *B. pricei* in having a fully ossified dorsal margin of the foramen magnum, and
470 an exit foramen for the occipital artery that is dorsal to the prootic foramen. The maxilla of
471 *Cretadhefdaa* is similar to *B. pricei* in having ornamentation on the lateral surface of the pars
472 facialis that extends ventrally to the pars dentalis, but differs in lacking a distinct palatine shelf.
473 *Cretadhefdaa* differs from *B. pricei* in having an occipital flange and a system of recesses on the
474 posterodorsal region of the braincase. *Cretadhefdaa* also differs from *B. pricei* in having more
475 slender and shorter neural spines on presacral vertebrae and slightly expanded sacral
476 transverse processes.

In his 2012 review, Agnolin described several specimens as *Calyptocephalella satan*, the oldest calyptocephalellid described (Agnolin, 2012). Although these specimens need to be reassessed (Báez and Gómez, 2018) and likely represent more than one taxon (Muzzopappa et al., 2020), their attribution to Calyptocephalellidae is certain. *Cretadhefdaa* resembles *C. satan* in having dermal skull bones covered with an ornamentation of pits and ridges, but differs in lacking a distinct palatine shelf (all calyptocephalellids exhibit a distinct palatine shelf; Muzzopappa and Báez, 2009; Agnolin, 2012), in having fused frontoparietals without a medial suture, and in having an occipital flange on the frontoparietals (Fig. 1A). The postcranial elements of *Cretadhefdaa* resemble *C. satan* in having procoelous vertebrae with anteroposteriorly elongate centra for the anterior presacral vertebrae, and shorter centra for posterior presacral and sacral vertebrae (Agnolin, 2012). The sacral vertebra bears a bicondylar articulation in both taxa, but *Cretadhefdaa* differs in having sacral transverse processes that are weakly expanded distally, whereas *C. satan* exhibits greatly expanded sacral transverse processes (Agnolin, 2012: fig. 10A, B) .

One last ornamented Cretaceous neobatrachian taxon is *Hungarobatrachus szukacsi* Szentesi & Venczel, 2010 from the Late Cretaceous of Hungary. Its vertebral elements are not known, but several skull fragments were recently described (Venzcel et al., 2021). Both taxa have fused frontoparietals without a trace of suture along their medial margin. However, *Cretadhefdaa* differs from *H. szukacsi* in having a system of recesses on each side of the posterior surface of its frontoparietals (divided by the posterior process) with the foramen for the occipital artery opening in a deep recess and an occipital flange on the frontoparietals. In *H. szukacsi*, the posterior surface of the frontoparietals is smooth with a slight depression and the foramen for

499 the occipital artery opens on each side of the posterior process (Venczel et al., 2021: fig.3) . The
500 frontoparietals of *H. szukacsi* also bear an incrassatio frontoparietalis on the ventral surface
501 whereas *Cretadhefdaa* does not. The maxilla of *Cretadhefdaa* differs from that of *H. szukacsi* in
502 lacking a distinct palatine shelf (Venczel et al., 2021: fig. 5).

503 **Comparison to hyperossified extinct ranoids**

504 Two other hyperossified taxa are relevant for comparisons to *Cretadhefdaa*: *Rocekophryne*
505 *ornata* Rage et al. 2021 from the Early Eocene of Algeria (Rage et al., 2021) and
506 *Thaumastosaurus servatus* Filhol 1877 from the Middle to Late Eocene of southwestern France
507 (Lemierre et al., 2021). These are the oldest occurrences of ornamented ranoids in the fossil
508 record (Lemierre et al., 2021; Rage et al., 2021).

509 *Rocekophryne ornata* is known from fragmentary cranial and postcranial remains. *Cretadhefdaa*
510 resembles *Rocekophryne* in having fused frontoparietals without a median suture and bearing
511 an ornamentation of pits and ridges, an occipital flange, and in lacking an incrassatio
512 frontoparietalis on the ventral surface of the frontoparietals. In addition, *Cretadhefdaa* and
513 *Rocekophryne* both bear ornamentation on the lateral surface of the pars facialis of the maxilla
514 that extends ventrally to the pars dentalis (Fig. 3F). However, *Cretadhefdaa* differs in lacking a
515 lateral flange on the posterior surface of the frontoparietal, lacking a distinct palatine shelf, and
516 in having very short processes paraoccipitalis (well-developed in *Rocekophryne*; Rage et al.,
517 2021: fig. 3A—F) and a series of recesses on the posterodorsal surface of the braincase. In
518 addition, the sacral vertebra of *Rocekophryne* bears an anterior condyle (instead of an anterior
519 cotyle in *Cretadhefdaa*) that indicates that the vertebral column is diplasiocoelous (Rage et al.,

2021: fig. 4A, B) and possesses transverse processes that are circular in lateral view (not circular in *Cretadhefdaa*).

Thaumastosaurus servatus is known from fragmentary remains and three partially complete and articulated skeletons (Rage and Roček, 2007; Lemierre et al., 2021). As with *R. ornata*, *Cretadhefdaa* and *T. servatus* have fused and ornamented frontoparietals without a medial suture. The anterior surface of the prooticooccipitals of both taxa exhibit a well-delimited but shallow and narrow groove for the jugular vein (Rage and Roček, 2007: fig. 7; Lemierre et al., 2021: fig. 8F). However, *Cretadhefdaa differs* from *T. servatus* in having an occipital flange and reduced processes paraoccipitalis*,* lateromedially compressed occipital condyles (instead of crescent shaped), and a series of recesses in the posterodorsal surface of the braincase (Fig. 1). *Cretadhefdaa* also differs from *T. servatus* in lacking a single, tapered posterior process of the parasphenoid and an incrassatio frontoparietalis on the ventral surface of the frontoparietals (Fig. 1C). In addition, the vertebral column of *T. servatus* is diplasiocoelous instead of procoelous as in *Cretadhefdaa*.

Comparisons to extant hyperossified hyloids

Cretadhefdaa shares numerous characters with ornamented extant Neobatrachia. Most of these similarities are associated with hyperossification, but two characters deserve further attention. The first is the presence of contact between the squamosal and frontoparietals, which occurs frequently (but not uniquely) in Hyloides (e.g., Calyptocephalellidae, Ceratophryidae, or the hylid *Triprion*). The second is the series of recesses on the posterodorsal surface of the braincase in *Cretadhefdaa*. This is known only in *Beelzebufo* and in *Ceratophrys*

(Evans et al., 2014; Fig. 5B, C). However, both *Cretadhefdaa* and *Beelzebufo* differ from *Ceratophrys* in having the foramen for the occipital artery located in the central recess, whereas it is found in the medial recess in extant taxa (Fig. 5). The braincase of *Ceratophrys* is similar to *Cretadhefdaa* in having fused frontoparietals, no distinct posterior process, and barely distinct processes paraoccipitalis. *Cretadhefdaa* differs from *Ceratophrys* in having an occipital flange, a well-delimited groove for the jugular vein, and in lacking the expanded "table" atop the neural spine of presacral vertebrae. The extant *Triprion* and *Diaglena* differ from *Cretadhefdaa* in having a frontoparietal extending posteriorly up to the end of the epiotic eminence, covering it dorsally. *Triprion* also lacks the system of recesses on the posterodorsal surface of the braincase. *Diaglena* bears recesses on it posterodorsal region of the braincase, but differs from *Cretadhefdaa* in having the foramen for the occipital artery not located within a recess.

NEOBATRACHIA? Reig, 1958

RANOIDES? Frost et al., 2006

Forelimb (UCRC-PV104)

This specimen is an incomplete humerus missing it proximal end and part of the diaphysis (Fig. 6). The diaphysis is straight, and a thin ventral ridge on the proximal end of the bone extends distally to the midlength of the diaphysis (Fig. 6A, C). The fossa cubitalis is very reduced, being shallow and not well-delimited, and visible in ventral view only as a thin crescent around the humeral head (Fig. 6A). The humeral head is large and in-line with the main axis of the diaphysis. The epicondyles are not symmetrical, with the ulnar epicondyle well-developed and

562 the radial epicondyle reduced and barely visible in ventral view (Fig. 6A). In dorsal view, the
563 olecranon scar is short, with a tapered and pointed end (Fig. 6B).

564 **Comparisons**

565 The combination of a large humeral head and asymmetrically developed epicondyles is
566 diagnostic for most Neobatrachia (Prasad and Rage, 2004; Rage et al., 2013), although this
567 combination of characters has not been evaluated in phylogenetic analyses. The presence of a
568 straight diaphysis, a humeral head in line with the axis of the diaphysis, and a shallow, poorly
569 delimited fossa cubitalis are found in most ranoids (Rage et al., 2013; de Lapparent de Broin et
570 al., 2020). It differs from the humerus of *Thaumastosaurus servatus* Filhol, 1877, one of the
571 earliest known ranoids, in having a crescent-shaped fossa cubitalis (triangular in *T. servatus*)
572 and a less developed ulnare epicondyle. Among the Cretaceous neobatrachian taxa, only
573 *Eurycephalella alcinae* Báez et al. 2009 and *Arariphrynus placidoi* Leal and Brito 2006 have
574 preserved humeri with their ventral surface exposed. The humerus of *A. placidoi* differs from
575 UCRC-PV104 in having two well-developed epicondyles (instead of a reduced radial epicondyle)
576 and a deep fossa cubitalis (instead of a shallow fossa in UCRC-PV104).

577 These comparisons suggest that UCRC-PV104 should be referred to the Neobatrachia. UCRC-
578 PV104 shares several characters with extant and extinct Ranoides, as well as with the oldest
579 (putative) member of the Ranoides (*Thaumastosaurus servatus*). However, because no
580 phylogenetic analyses have yet shown synapomorphies for Ranoides related to the humerus,
581 we refer this fossil to the Neobatrachia and recognize the assignment to Ranoides as tentative.

582

583 INCERTAE SEDIS

584 **Pelvic girdle (UCRC-PV105)**

585 This element is an incomplete left ilium, preserving most of its acetabular region. UCRC-PV105
586 bears a high and well-developed dorsal crest, although its extension on the ilial shaft is
587 unknown (Fig. 7I J). The dorsal crest appears to be lacking its dorsalmost portion, indicating
588 that it was more extensive (Fig. 7I, K). The dorsal prominence is low and elongate
589 anteroposteriorly, and the dorsal protuberance is strongly oriented laterally (Fig. 7K). The
590 acetabular rim is well developed on its ventral region. Although not complete, both the dorsal
591 and ventral acetabular expansions are developed. The dorsal acetabular expansion is inclined
592 posteromedially (Fig. 7I). Although poorly preserved, the ventral acetabular expansion was
593 well-developed, extending ventrally (Fig. 4I). The preacetabular angle is obtuse and the
594 preacetabular zone is narrow (Fig. 7I). In medial view, a shallow but well delimited medial ridge
595 is present, starting from the base or the dorsal acetabular expansion to the anteriormost
596 preserved portion (Fig. 7J). In posterior view, the ilioischiatic juncture is moderately wide and
597 an interiliac tubercle is absent (Fig. 7L).

598 **Comparisons**

599 Ilia are one of the most common anuran elements recovered in the fossil record (Roček, 2000;
600 Rage and Roček, 2003; Roček, 2013; Gardner and Rage, 2016) and several authors have
601 proposed characters to identify the ilia of the different clades (Gardner et al., 2010; Gómez and
602 Turazzini, 2016; Matthews et al., 2019). However, these are largely based on extant anurans
603 and can be difficult to apply to Mesozoic anurans (Roček et al., 2010; Roček, 2013). The

presence of a well-developed dorsal crest is found in several clades (Alytoidea, Pipoidea, and Neobatrachia, especially Ranoides), but likely reflects similarity in locomotion rather than close phylogenetic relationships (Roček, 2013). The absence of an interiliac tubercle is diagnostic for many neobatrachians, with notable exceptions such as *H. szukacsi* and the aquatic hylid *Pseudis* (Gómez and Turazzini, 2016; Venczel et al., 2021). However, the utility of this character has not been tested thoroughly in a taxon-rich phylogenetic analysis (Gómez and Turazzini, 2016). Agnolin (2012) argued that the presence of a broad preacetabular zone and large acetabular fossa was diagnostic for the Calyptocephalellidae but this was not evaluated in a phylogenetic analysis and may represent an example of convergent evolution. There are no characters that allow for a precise attribution of this ilium (UCRC-PV105) to the other anurans from the Kem Kem or other specific anuran lineages.

Phylogenetic Analyses

Recent phylogenetic analyses (Báez and Gómez, 2018; Lemierre et al., 2021) are based on a similar dataset. This dataset was first elaborated by Báez et al. (2009), based on the dataset of Fabrezi (2006) that was developed for a phylogenetic analysis of ceratophryids. The dataset from Báez et al. (2009) includes 42 taxa—three of which are extinct taxa—and 75 characters. In a separate analysis, Báez and Gómez (2018) modified the dataset from Fabrezi (2006) further by adding 29 neobatrachian taxa and redefining some characters to test the impact of characters related to hyperossification. They expanded the taxon sampling to 71 taxa and added 68 characters (for a total of 143 characters), as well as redefined several characters.

Finally, Lemierre et al. (2021) further enlarged the dataset from Báez and Gomez (2018), by adding 15 extant natatanuran ranoid taxa (for a total of 20 natatanuran taxa). The vast majority of extant anurans belong to the Neobatrachia (Feng et al., 2017), which includes two large clades, the Hyloides and the Ranoides. To date, phylogenetic analyses based solely on morphological characters (e.g., Scott, 2005) do not recover many of the clades found in recent molecular phylogenetic analyses (e.g., Roelants et al. 2007; Feng et al., 2017; Jetz and Pyron, 2018; Hime et al. 2021). To evaluate the phylogenetic placement of *Cretadhefdaa,* we analyzed our character matrix using different sets of assumptions as well as one analysis using a constraint tree reflecting recent results from molecular phylogenetic analyses.

Results

We obtained 60 MPTs (most parsimonious trees) of 1362 steps (CI = 0.139; RI = 0.418) with the analysis performed under equal weight with cline characters ordered. The strict consensus (Fig. 7) shows large polytomies, and the monophyly of the Neobatrachia is not recovered. This seems to be linked to the uncertainties regarding the position of *Arariphrynus placidoi*, and the lack of characters scored for *Cretadhefdaa* and *Hungarobatrachus szukacsi* (13 and 11% of characters scored, respectively). *Cretadhefdaa* is recovered within a clade containing *Uberabatrachus* and the Ceratophryoidea. This clade is supported by three synapomorphies, all of which are character states found in other groups of frogs: (1) a position of articulation of lower jaw and skull at the level of occiput (character 61: 0 >1); (2) cotyle of the atlas widely separated (76: 1 >2) and (3) angle between iliac shaft and ventral acetabular expansion obtuse (125: 1 >2). *Cretadhefdaa* is placed within this clade in a polytomy with the Ceratophryidae.

This clade is supported by five synapomorphies mainly related to hyperossified cranial characters (see Appendix S4 in Supplemental Data 1).

When excluding *Arariphrynus*, we obtained 10 trees of 1355 steps. The strict consensus (CI = 0.174; RI = 0.556; Fig. 8) shows a trichotomy with Pelobatoidae, *Heleophryne*, and the remaining Neobatrachia. The 'Neobatrachia' (the clade exclusive of *Heleophryne*) is supported by a five synapomorphies: (1) otic plate of the squamosal short, overlapping only the most lateral portion of the crista parotica (9: 0 >1); (2) absence of process or crest on the anterior margin of the scapula (114: 3 >0); (3) configuration of the postaxial carpals as ulnare free, 3+4+5 (119: 0 >2); (4) well developed posterodorsal expansion of the ischium (131: 0 >1) and (5) horizontal pupil shape (143: 0 >2). Among the Neobatrachia, we recovered a large hyperossified clade, supported by six synapomorphies (see Appendix S4 in Supplemental Data 1). *Hungarobatrachus* is within a poorly supported trichotomy with *Eurycephalella* and *Calyptocephalella*, for which there are three synapomorphies: (1) contact between lamella alaris of the squamosal and frontoparietals on the dorsal surface of the otic capsule (8: 0 >2); (2) anterior ramus of the pterygoid not reaching planum anteorbitale (12: 0 >1) and (3) postaxial carpal with ulnare and 3 free (119: 2 >1). *Cretadhefdaa* is recovered within a large polytomy with extant Ceratophryidae, poorly supported by four synapomorphies (see Appendix S4 in Supplemental Data 1).

In analyses using a topological constraint (and excluding *Arariphrynus placidoi*), we obtained 190 trees, with a score of 1395 steps. The strict consensus (CI = 0. 126, RI = 0. 247; Fig. 9) shows

667 a monophyletic Neobatrachia, Ranoides, and Hyloides, but all of the monophyly of each was
668 enforced in the constraint tree. Within Hyloides, most taxa are placed within a large unresolved
669 clade (Fig. 9). *Cretadhefdaa* is recovered in a large polytomy within Hyloides as are
670 *Baurubatrachus*, *Beelzebufo*, *Cratia*, *Eurycephalella*, *Hungarobatrachus*, and *Uberabatrachus*.
671 The only extinct taxon to be recovered elsewhere in the phylogeny is *Thaumastosaurus*, which
672 is recovered in a clade of Ranoides with *Aubria*, *Cornufer*, and *Pyxicephalus*.

673

674 Discussion

675 ***Phylogenetic analyses***

676 The poor resolution of the topology obtained when performing phylogenetic analysis under
677 equal weights is not surprising. *Hungarobatrachus szukacsi* has only 16 scored characters within
678 the dataset, none of which are clear neobatrachian synapomorphies, and the skeleton of
679 *Arariphrynus* is very incomplete leading to few scored characters, in peculiar regarding pectoral
680 girdle and vertebrae (51 scored characters in total; see Baez et al., 2009). In addition, most of
681 the scored cranial characters for *Hungarobatrachus* and *Cretadhefdaa* are linked to
682 hyperossification, a recurrent feature in anuran evolution (see above) that likely obscures the
683 phylogenetic relationships of *Cretadhefdaa.* One putative synapomorphy of Neobatrachia, the
684 presence of palatine, is inferred in *Cretadhefdaa* (27: 1). When performing the analysis with this
685 character considered as unknown (27: ?), the position of *Cretadhefdaa* does not change (data
686 not shown).

687 The phylogenetic positions of *Cretadhefdaa* and *Hungarobatrachus* are similar to several
688 hyperossified extinct Cretaceous taxa by being close to either the Ceratophryidae or
689 Calyptocephalellidae. Recent analyses (Báez and Gómez, 2018) have highlighted that
690 convergence due to hyperossification likely plays a role in the position recovered for other
691 hyperossified extinct neobatrachian taxa. This could influence the position of *Cretadhefdaa* as
692 well. Nevertheless, the combination of characters of *Cretadhefdaa* confirms its assignment to
693 Neobatrachia. In addition, one character mentioned in the description of the braincase, the
694 presence of a series of recesses in posterodorsal region of the braincase, deserves attention. In
695 addition to *Cretadhefdaa,* a similar (but not clearly homologous) morphology has only been
696 identified in *Beelzebufo* and in the Ceratophryidae (except in *Chacophrys*). To our knowledge,
697 this character has not been used in phylogenetic analyses (e.g., Gómez and Turazzini, 2021).
698 However, the two extant taxa possessing these recesses are closely related (*Ceratophrys* and
699 *Lepidobatrachus*), and the extinct *Beelzebufo* has been proposed as a stem member of the
700 Ceratophryidae (Báez and Gómez, 2018; Lemierre et al., 2021). Interestingly, *Cretadhefdaa* is
701 recovered in a more crownward position within Ceratophryidae than *Beelzebufo*, even in other
702 analyses (Báez and Gómez, 2018; Lemierre et al., 2021). It is necessary to test the phylogenetic
703 significance of this character to confirm this hypothesis, which is beyond the scope of this
704 paper. When using a topological constraint based on recent phylogenomic analyses, most
705 extinct taxa—including *Cretadhefdaa*—included in the analysis were recovered as part of
706 Hyloides, though as part of a large polytomy. In conclusion, our phylogenetic analyses point to
707 *Cretadhefdaa* being within the Neobatrachia, even if most of the synapomorphies diagnostic of
708 this clade are not scored, and several analyses support a hyloid affinity.

709

710 ***Paleobiogeographical implications***

711 Neobatrachians are known in the fossil record during the Late Cretaceous from three main
712 locations: Madagascar (Maastrichtian; Evans et al., 2014), Europe (Campanian; Venczel et al.,
713 2021), and South America (Maastrichtian; Báez and Gómez, 2018). The South American fossil
714 record is of particular importance with numerous taxa known from articulated specimens (Báez
715 et al., 2009; Báez and Gómez, 2018; Agnolin et al., 2020; Moura et al., 2021). In contrast, only
716 fragmentary remains of two taxa have been recovered from Madagascar and Europe (Evans et
717 al., 2008; 2014; Venczel et al., 2021). There are other reports of neobatrachians from the
718 Cretaceous (Báez and Werner, 1996; Prasad and Rage, 2004; Rage, 1984; Rage et al., 2020) but
719 the attribution of these to the Neobatrachia remains uncertain because diagnostic elements are
720 often not preserved and these other fossils have not been included in phylogenetic analyses.
721 Because *Cretadhefdaa* is from the Mid-Cenomanian, it is the oldest neobatrachian of Africa.

722 The oldest occurrence of the Neobatrachia is from the Brazilian Crato Formation (Leal and Brito,
723 2006; Báez et al., 2009; Agnolin et al., 2020; Moura et al., 2021), which preserves extinct
724 anurans from the Aptian (Early Cretaceous). However, *Cretadhefdaa* is still the oldest
725 occurrence of Neobatrachia outside of South America. The Neobatrachia began to diversify
726 during the earliest Cretaceous, including an early split into two major lineages, Hyloides and
727 Ranoides, each of which was largely restricted to a portion of western Gondwana, respectively,
728 South America and Africa (Frazão et al., 2015; Feng et al., 2017). Time-calibrated molecular
729 phylogenetic analyses (e.g., Feng et al., 2017) suggest that by 96–95 Ma (i.e., the period from

730 which *Cretadhefdaa* was recovered), the Neobatrachia was already separated into a number of
731 lineages that are restricted today to specific biogeographic regions. These include the
732 Myobatrachidae of Australia, the hyloids of South America, the Microhylidae (widespread today
733 across the tropics), the Afrobatrachia of sub-Saharan Africa, the natatanuran ranoids, and the
734 lineage leading to the Sooglossidae and Nasikabatrachidae that are today restricted,
735 respectively, to the Seychelles Islands and the Western Ghats of India. There remains ample
736 opportunity for both additional sampling and study of neobatrachian fossils from Gondwanan
737 landmasses that could add new insights into the early evolution and biogeography of these
738 major extant frog lineages that diversified in the Early Cretaceous.

739 The current absence of Ranoides from the Cretaceous fossil record is puzzling. Except for
740 undescribed and unillustrated material that was attributed to Ranoides two decades ago (Báez
741 and Werner, 1996), there is surprisingly few ranoid fossils especially in comparison to the hyloid
742 fossils discovered in South America, Europe, and Africa. Their absence could be due to several
743 factors. The first and most obvious is the lack of anuran specimens from the fossil record of
744 Africa, due both to a lack of targeted collecting and little academic research on existing
745 material. One example that highlights this problem is the Pyxicephalidae, a clade of ranoids
746 endemic to Africa (Channing and Rödel, 2019) and for which time-calibrated molecular
747 phylogenetic analyses suggest a divergence from other natatanurans around 60 Ma (Early
748 Palaeocene). Yet, the oldest occurrence of this family is *Thaumastosaurus* from the Middle-Late
749 Eocene of Europe, whereas the earliest African fossil is from only 5 Ma (Matthews et al., 2015;
750 Lemierre et al., 2021). The large gap in the fossil record of this family is found in many other
751 families of Ranoides, and many clades with an African origin completely lack a fossil record.

Another bias could be that the vast majority of Ranoides are not hyperossified anurans, including many small-sized species, and thus less likely to be preserved as intact and diagnosable fossils. In addition, numerous synapomorphies of Ranoides are for postcranial elements, such as the vertebrae and the pectoral girdle, that are less likely to be identified and/or preserved (Scott, 2005; Frost et al., 2006). A final bias is simply that there has been sustained interest from South American paleontologists in the fossil record of anurans from countries such as Bolivia, Brazil, and Argentina, whereas there have been exceedingly few African paleontologists dedicated to studying anurans.

Conclusion

Our study confirms the report of Rage and Dutheil (2008) that at least three anuran taxa are present in the Kem Kem beds of Morocco. The newly described *Cretadhefdaa taouzensis* can be attributed to the Neobatrachia, making it both the oldest occurrence of the clade outside of South America and only the second occurrence in the Cretaceous of Africa. Several postcranial bones also point to an affinity with the Neobatrachia but cannot be associated definitively with either *Cretadhefdaa* or another taxon. The presence of a neobatrachian in the Kem Kem in the Cenomanian demonstrates that neobatrachians were already widespread on Gondwana during the earliest Late Cretaceous.

Acknowledgement

We thank Paul Sereno (University of Chicago) for access to and loan of the specimens, and Edward Stanley (University of Florida) for CT-scanning them. Processing of tomographic data was undertaken at the 3D imaging facilities Lab of the UMR 7207 CR2P (MNHN CNRS UPMC, Paris). We thank María Vallejo-Pareja for comments on a draft of this manuscript.

References

Agnolin F. 2012. A New Calyptocephalellidae (anura, Neobatrachia) from the Upper Cretaceous of Patagonia, Argentina, with Comments on Its Systematic Position. *Studia Geologica Salmanticensia* 48:129–178.

Agnolin F, Carvalho I de S, Aranciaga Rolando AM, Novas FE, Xavier-Neto J, Andrade JAFG, Freitas FI. 2020. Early Cretaceous neobatrachian frog (Anura) from Brazil sheds light on the origin of modern anurans. *Journal of South American Earth Sciences* 101:102633. DOI: 10.1016/j.jsames.2020.102633.

Báez AM, Gómez RO. 2018. Dealing with homoplasy: osteology and phylogenetic relationships of the bizarre neobatrachian frog *Baurubatrachus pricei* from the Upper Cretaceous of Brazil. *Journal of Systematic Palaeontology* 16:279–308. DOI: 10.1080/14772019.2017.1287130.

Báez AM, Gómez RO, Ribeiro LCB, Martinelli AG, Teixeira VPA, Ferraz MLF. 2012. The diverse Cretaceous neobatrachian fauna of South America: *Uberabatrachus carvalhoi*, a new frog from the Maastrichtian Marília Formation, Minas Gerais, Brazil. *Gondwana Research* 22:1141–1150. DOI: 10.1016/j.gr.2012.02.021.

792 Báez AM, Moura GJB, Gómez RO. 2009. Anurans from the Lower Cretaceous Crato Formation of
793 northeastern Brazil: implications for the early divergence of neobatrachians. *Cretaceous*
794 *Research* 30:829–846. DOI: 10.1016/j.cretres.2009.01.002.

795 Báez AM, Perí S. 1989. *Baurubatrachus pricei*, nov. gen. et sp., un Anuro del Cretacico Superior
796 de Minas Gerais. *Anais da Academia Brasileira de Ciências* 61:447–458.

797 Báez AM, Rage J-C. 1998. Pipid frogs from the Upper Cretaceous of In Beceten, Niger.
798 *Palaeontology* 41:669–691.

799 Báez AM, Werner C. 1996. Presencia de Anuros Ranoideos en el Cretácico de Sudan.
800 *AMEGHINIANA* 33:460.

801 Biton R, Boistel R, Rabinovich R, Gafny S, Brumfeld V, Bailon S. 2016. Osteological observations
802 on the Alytid Anura *Latonia nigriventer* with comments on functional morphology,
803 biogeography, and evolutionary history. *Journal of Morphology* 277:1131–1145. DOI:
804 10.1002/jmor.20562.

805 Blakey RC. 2008. Gondwana paleobiogeography from assembly to breakup—A 500 m.y.
806 odyssey. In: Fielding CR, Frank TD, Isbell JL eds. *Resolving the Late Paleozoic Ice Age in time and*
807 *space*. The Geological Society of America Special Paper. Boulder, CO, USA: The Geological
808 Society of America, 1–28.

809 de Broin F, Buffetaut E, Koeniger J-C, Rage J, Russell D, Taquet P, Vergnaud-Grazzini C, Wenz S.
810 1974. La faune de vertébrés continentaux du gisement d'In Betceten (Sénonien du Niger).
811 *Comptes Rendus de l'Académie des Sciences, Paris* 279:439–472.

812 Cavin L, Tong H, Boudad L, Meister C, Piuz A, Tabouelle J, Aarab M, Amiot R, Buffetaut E, Dyke
813 G, Hua S, Le Loeuff J. 2010. Vertebrate assemblages from the early Late Cretaceous of
814 southeastern Morocco: An overview. *Journal of African Earth Sciences* 57:391–412. DOI:
815 10.1016/j.jafrearsci.2009.12.007.

816 Channing A, Rödel M-O. 2019. *Field Guide to the Frogs & Other Amphibians of Africa*. Penguin
817 Random House South Africa.

818 Duellman WE, Trueb L. 1994. *Biology of Amphibians*. JHU Press.

819 Dutheil DB. 1999. An overview of the freshwater fish fauna from the Kem Kem beds (Late
820 Cretaceous: Cenomanian) of southesatern Morocco. In: Arrratia G, Schultze HP eds. *Mesozoic*
821 *fishes-Systematics and fossil record*. Munich: F. Pfeil, 553–563.

822 Ettachfini EM, Andreu B. 2004. Le Cénomanien et le Turonien de la Plate-forme Préafricaine du
823 Maroc. *Cretaceous Research* 25:277–302. DOI: 10.1016/j.cretres.2004.01.001.

824 Evans SE, Groenke JR, Jones MEH, Turner AH, Krause DW. 2014. New Material of *Beelzebufo* , a
825 Hyperossified Frog (Amphibia: Anura) from the Late Cretaceous of Madagascar. *PLoS ONE*
826 9:e87236. DOI: 10.1371/journal.pone.0087236.

827 Evans SE, Jones MEH, Krause DW. 2008. A giant frog with South American affinities from the
828 Late Cretaceous of Madagascar. *Proceedings of the National Academy of Sciences* 105:2951–
829 2956. DOI: 10.1073/pnas.0707599105.

Fabrezi M. 2006. Morphological evolution of Ceratophryinae (Anura, Neobatrachia). *Journal of Zoological Systematics and Evolutionary Research* 44:153–166. DOI: 10.1111/j.1439-0469.2005.00349.x.

Feng Y-J, Blackburn DC, Liang D, Hillis DM, Wake DB, Cannatella DC, Zhang P. 2017. Phylogenomics reveals rapid, simultaneous diversification of three major clades of Gondwanan frogs at the Cretaceous–Paleogene boundary. *Proceedings of the National Academy of Sciences* 114:E5864–E5870. DOI: 10.1073/pnas.1704632114.

Filhol H. 1877. *Recherches sur les phosphorites du Quercy: Etude des fossiles qu'on y rencontre et spécialement des mammifères*. Paris.

Frazão A, Silva HR da, Russo CA de M. 2015. The Gondwana Breakup and the History of the Atlantic and Indian Oceans Unveils Two New Clades for Early Neobatrachian Diversification. *PLOS ONE* 10:e0143926. DOI: 10.1371/journal.pone.0143926.

Frishkopf LS, Goldstein MH. 1963. Responses to Acoustic Stimuli from Single Units in the Eighth Nerve of the Bullfrog. *The Journal of the Acoustical Society of America* 35:1219–1228. DOI: 10.1121/1.1918676.

Frost DR, Grant T, Faivovich J, Bain RH, Haas A, Haddad CFB, De Sá RO, Channing A, Wilkinson M, Donnellan SC, Raxworthy CJ, Campbell JA, Blotto BL, Moler P, Drewes RC, Nussbaum RA, Lynch JD, Green DM, Wheeler WC. 2006. The Amphibian Tree of Life. *Bulletin of the American Museum of Natural History* 297:1–291. DOI: 10.1206/0003-0090(2006)297[0001:TATOL]2.0.CO;2.

850 Gardner JD, Rage J-C. 2016. The fossil record of lissamphibians from Africa, Madagascar, and
851 the Arabian Plate. *Palaeobiodiversity and Palaeoenvironments* 96:169–220. DOI:
852 10.1007/s12549-015-0221-0.

853 Gardner JD, Roček Z, Přikryl T, Eaton JG, Blob RW, Sankey JT. 2010. Comparative morphology of
854 the ilium of anurans and urodeles (Lissamphibia) and a re-assessment of the anuran affinities of
855 *Nezpercius dodsoni* Blob et al., 2001. *Journal of Vertebrate Paleontology* 30:1684–1696. DOI:
856 10.1080/02724634.2010.521605.

857 Gaupp E. 1896. *Anatomie des Frosches. Pt. 3*. Braunschweg: Friedrich Vieweg Und Shon.

858 Goloboff PA, Catalano SA. 2016. TNT version 1.5, including a full implementation of
859 phylogenetic morphometrics. *Cladistics* 32:221–238. DOI: 10.1111/cla.12160.

860 Gómez RO, Turazzini GF. 2016. An overview of the ilium of anurans (Lissamphibia, Salientia),
861 with a critical appraisal of the terminology and primary homology of main ilial features. *Journal*
862 *of Vertebrate Paleontology* 36:e1030023. DOI: 10.1080/02724634.2015.1030023.

863 Gómez RO, Turazzini GF. 2021. The fossil record and phylogeny of South American horned frogs
864 (Anura, Ceratophryidae). *Journal of Systematic Palaeontology* 0:1–52. DOI:
865 10.1080/14772019.2021.1892845.

866 Hime PM, Lemmon AR, Lemmon ECM, Prendini E, Brown JM, Thomson RC, Kratovil JD, Noonan
867 BP, Pyron RA, Peloso PLV, Kortyna ML, Keogh JS, Donnellan SC, Mueller RL, Raxworthy CJ, Kunte
868 K, Ron SR, Das S, Gaitonde N, Green DM, Labisko J, Che J, Weisrock DW. 2021. Phylogenomics

Reveals Ancient Gene Tree Discordance in the Amphibian Tree of Life. *Systematic Biology* 70:49–66. DOI: 10.1093/sysbio/syaa034.

Ibrahim N, Sereno PC, Varricchio DJ, Martill DM, Dutheil DB, Unwin DM, Baidder L, Larsson HCE, Zouhri S, Kaoukaya A. 2020. Geology and paleontology of the Upper Cretaceous Kem Kem Group of eastern Morocco. *ZooKeys* 928:1–216. DOI: 10.3897/zookeys.928.47517.

Jacobs LL, Winkler DA, Gomani EM. 1990. The Dinosaur Beds of northern Malawi, Africa. *National Geographic Research* 6:196–204.

Jetz W, Pyron RA. 2018. The interplay of past diversification and evolutionary isolation with present imperilment across the amphibian tree of life. *Nature Ecology & Evolution* 2:850–858. DOI: 10.1038/s41559-018-0515-5.

de Lapparent de Broin F, Bailon S, Augé ML, Rage J-C. 2020. Amphibians and reptiles from the Neogene of Afghanistan. *Geodiversitas* 42:409–426.

Leal MEC, Brito PM. 2006. Anura do Cretáceo Inferior da Bacia do Araripe, Nordeste do Brasil. In: Gallo V, Brito PM, Silva HMA, Figueiredo FJ eds. *Paleontología de Vertebrados. Grandes Temas e Contribuçoes Científicas*. Rio de Janeiro: Interciencia, 145–152.

Lemierre A, Folie A, Bailon S, Robin N, Laurin M. 2021. From toad to frog, a CT-based reconsideration of *Bufo servatus* , an Eocene anuran mummy from Quercy (France). *Journal of Vertebrate Paleontology* 41:e1989694. DOI: 10.1080/02724634.2021.1989694.

Maddin HC, Venczel M, Gardner JD, Rage J-C. 2013. Micro-computed tomography study of a three-dimensionally preserved neurocranium of *Albanerpeton* (Lissamphibia,

889 Albanerpetontidae) from the Pliocene of Hungary. *Journal of Vertebrate Paleontology* 33:568–
890 587. DOI: 10.1080/02724634.2013.722899.

891 Matthews T, van Dijk E, Roberts DL, Smith RMH. 2015. An early Pliocene (5.1 Ma) fossil frog
892 community from Langebaanweg, south-western Cape, South Africa. *African Journal of*
893 *Herpetology* 64:39–53. DOI: 10.1080/21564574.2014.985261.

894 Matthews T, Keeffe R, Blackburn DC. 2019. An identification guide to fossil frog assemblages of
895 southern Africa based on ilia of extant taxa. *Zoologischer Anzeiger* 283:46–57. DOI:
896 10.1016/j.jcz.2019.08.005.

897 McLoughlin S. 2001. The breakup history of Gondwana and its impact on pre-Cenozoic floristic
898 provincialism. *Australian Journal of Botany* 49:271. DOI: 10.1071/BT00023.

899 Moura PHAG, Costa FR, Anelli LE, Nunes I. 2021. A new genus of fossil frog (Anura) from lower
900 Cretaceous deposits in South America. *Anais da Academia Brasileira de Ciências* 93:e20191560.
901 DOI: 10.1590/0001-3765202120201560.

902 Muzzopappa P, Báez AM. 2009. Systematic status of the mid-Tertiary neobatrachian frog
903 Calyptocephalella canqueli from Patagonia (Argentina), with comments on the evolution of the
904 genus. *AMEGHINIANA* 46:113–125.

905 Muzzopappa P, Martinelli AG, Garderes JP, Rougier GW. 2020. Exceptional avian pellet from the
906 Paleocene of Patagonia and description of its content: a new species of calyptocephalellid
907 (Neobatrachia) anuran. *Papers in Palaeontology*:spp2.1333. DOI: 10.1002/spp2.1333.

Paluh DJ, Stanley EL, Blackburn DC. 2020. Evolution of hyperossification expands skull diversity in frogs. *Proceedings of the National Academy of Sciences* 117:8554–8562. DOI: 10.1073/pnas.2000872117.

Prasad GVR, Rage J-C. 2004. Fossil frogs (Amphibia: Anura) from the Upper Cretaceous intertrappean beds of Naskal, Andhra Pradesh, India. *Revue de Paléobiologie, Genève* 23:99–116.

Rage J-C. 1984. Are the Ranidae (Anura, Amphibia) known prior to the Oligocene? *Amphibia-Reptilia* 5:281–288. DOI: 10.1163/156853884X-005-03-09.

Rage J-C. 2008. Amphibia (Anura) from the Lower Miocene of the Sperrgebiet, Namibia. *Memoir of the Geological Survey of Namibia* 20:75–92.

Rage J-C, Adaci M, Bensalah M, Mahboubi M, Marivaux L, Mebrouk F, Tabuce R. 2021. Lastest Early-Middle Eocene deposits of Algeria (Glib Zegdou, HGL50) yield the richest and most diverse fauna of amphibians and squamate reptiles from the Palaeogene of Africa. *Paleovertebrata* 43.

Rage J-C, Dutheil DB. 2008. Amphibians and squamates from the Cretaceous (Cenomanian) of Morocco - A preliminary study, with description of a new genus of pipid frog. *Palaeontographica Abteilung A* 285:1–22. DOI: 10.1127/pala/285/2008/1.

Rage J-C, Pickford M, Senut B. 2013. Amphibians and squamates from the middle Eocene of Namibia, with comments on pre-Miocene anurans from Africa. *Annales de Paléontologie* 99:217–242. DOI: 10.1016/j.annpal.2013.04.001.

927 Rage J-C, Prasad GVR, Verma O, Khosla A, Parmar V. 2020. Anuran Lissamphibian and Squamate
928 Reptiles from the Upper Cretaceous (Maastrichtian) Deccan Intertrappean Sites in Central India,
929 with a Review of Lissamphibian and Squamate Diversity in the Northward Drifting Indian Plate.
930 In: Prasad GVR, Patnaik R eds. *Biological Consequences of Plate Tectonics*. Vertebrate
931 Paleobiology and Paleoanthropology. Cham: Springer International Publishing, 99–121. DOI:
932 10.1007/978-3-030-49753-8_6.

933 Rage J-C, Roček Z. 2003. Evolution of anuran assemblages in the Tertiary and Quaternary of
934 Europe, in the context of palaeoclimate and palaeogeography. *Amphibia-Reptilia* 24:133–167.
935 DOI: 10.1163/156853803322390408.

936 Rage J, Roček Z. 2007. A new species of *Thaumastosaurus* (Amphibia: Anura) from the Eocene
937 of Europe. *Journal of Vertebrate Paleontology* 27:329–336. DOI: 10.1671/0272-
938 4634(2007)27[329:ANSOTA]2.0.CO;2.

939 Rineau V, i Bagils RZ, Laurin M. 2018. Impact of errors on cladistic inference: simulation-based
940 comparison between parsimony and three-taxon analysis. *Contributions to Zoology* 87:25–40.
941 DOI: 10.1163/18759866-08701003.

942 Rineau V, Grand A, Zaragüeta R, Laurin M. 2015. Experimental systematics: sensitivity of
943 cladistic methods to polarization and character ordering schemes. *Contributions to Zoology*
944 84:129–148. DOI: 10.1163/18759866-08402003.

945 Roček Z. 1994. Taxonomy and Distribution of Tertiary Discoglossids (anura) of The Genus
946 *Latonia* V. Meyer, 1843. *Geobios* 27:717–751.

947 Roček Z. 2000. Mesozoic Anurans. In: Heatwole H, Carroll RL eds. *Palaeontology The*
948 *Evolutionnary History of Amphibians*. Amphibian BIology. 1295–1331.

949 Roček Z. 2008. The Late Cretaceous frog Gobiates from Central Asia: its evolutionary status and
950 possible phylogenetic relationships. *Cretaceous Research* 29:577–591. DOI:
951 10.1016/j.cretres.2008.01.005.

952 Roček Z. 2013. Mesozoic and Tertiary Anura of Laurasia. *Palaeobiodiversity and*
953 *Palaeoenvironments* 93:397–439. DOI: 10.1007/s12549-013-0131-y.

954 Roček Z, Eaton JG, Gardner JD, Přikryl T. 2010. Evolution of anuran assemblages in the Late
955 Cretaceous of Utah, USA. *Palaeobiodiversity and Palaeoenvironments* 90:341–393.

956 Roček Z, Wuttke M, Gardner JD, Singh Bhullar B-A. 2014. The Euro-American genus
957 *Eopelobates*, and a re-definition of the family Pelobatidae (Amphibia, Anura). *Palaeobiodiversity*
958 *and Palaeoenvironments* 94:529–567. DOI: 10.1007/s12549-014-0169-5.

959 Roelants K, Gower DJ, Wilkinson M, Loader SP, Biju SD, Guillaume K, Moriau L, Bossuyt F. 2007.
960 Global patterns of diversification in the history of modern amphibians. *Proceedings of the*
961 *National Academy of Sciences* 104:887–892. DOI: 10.1073/pnas.0608378104.

962 Scott E. 2005. A phylogeny of ranid frogs (Anura: Ranoidea: Ranidae), based on a simultaneous
963 analysis of morphological and molecular data. *Cladistics* 21:507–574. DOI: 10.1111/j.1096-
964 0031.2005.00079.x.

965 Sereno PC, Dutheil DB, Iarochene M, Larsson HCE, Lyon GH, Magwene PM, Sidor CA, Varricchio
966 DJ, Wilson JA. 1996. Predatory Dinosaurs from the Sahara and Late Cretaceous Faunal
967 Differentiation. *Science* 272:986–991. DOI: 10.1126/science.272.5264.986.

968 Streicher, J.W., Miller, E.C., Guerrero, P.C., Correa, C., Ortiz, J.C., Crawford, A.J., Pie, M.R. and
969 Wiens, J.J., 2018. Evaluating methods for phylogenomic analyses, and a new phylogeny for a
970 major frog clade (Hyloidea) based on 2214 loci. *Molecular Phylogenetics and Evolution*,
971 119:128-143.

972 Szentesi Z, Venczel M. 2010. An advanced anuran from the Late Cretaceous (Santonian) of
973 Hungary. *Neues Jahrbuch für Geologie und Paläontologie - Abhandlungen* 256:291–302. DOI:
974 10.1127/0077-7749/2010/0054.

975 Trueb L. 1973. Bones, Frogs and Evolution. In: Vial JL ed. *Evolutionary Biology of the Anurans.*
976 *Contemporary Research on Major Problems*. Columbia: University of Missouri Press, 65–133.

977 Trueb L, Púgener LA, Maglia AM. 2000. Ontogeny of the bizarre: an osteological description of
978 *Pipa pipa* (Anura: Pipidae), with an account of skeletal development in the species. *Journal of*
979 *Morphology* 243:75–104. DOI: 10.1002/(SICI)1097-4687(200001)243:1<75::AID-
980 JMOR4>3.0.CO;2-L.

981 Venczel M, Szentesi Z, Gardner JD. 2021. New material of the frog *Hungarobatrachus szukacsi*
982 Szentesi & Venczel, 2010, from the Santonian of Hungary, supports its neobatrachian affinities
983 and reveals a Gondwanan influence on the European Late Cretaceous anuran fauna.
984 *Geodiversitas* 43. DOI: 10.5252/geodiversitas2021v43a7.

985 Wever EG. 1979. Middle ear muscles of the frog. *Proceedings of the National Academy of*
986 *Sciences* 76:3031–3033. DOI: 10.1073/pnas.76.6.3031.

987 Wever EG. 1985. *The Amphibian Ear*. Princeton, New Jeresy, USA: Princeton University Press.

988 Yuan, Z.Y., Zhang, B.L., Raxworthy, C.J., Weisrock, D.W., Hime, P.M., Jin, J.Q., Lemmon, E.M.,
989 Lemmon, A.R., Holland, S.D., Kortyna, M.L. and Zhou, W.W., 2018. Natatanuran frogs used the
990 Indian Plate to step-stone disperse and radiate across the Indian Ocean. *National Science*
991 *Review*, 6:10-14.

992 Zouhri S (ed.). 2017. *Paléontologie des vertébrés du Maroc: état des connaissances*. Paris.

993

Figure 1

UCRC-PV64, holotype of *Cretadhefdaa*

Incomplete braincase in **A** dorsal; **B** ventral; **C** anterior; **D** posterior; **E** left lateral; and **F** left medial views. Same specimen in **G** posterodorsal view with a close up on the recesses system. **Abbreviations**: **acf?**, fused acoustic foramina; **cc**, carotid canal; **cdf**, condyloid fossa; **cltp**, cultriform process; **cr?**, central recess; **ee**, epiotic eminence; **efca**, exit foramen for the carotid artera; **fm**, foramen magnum; **gr.jv**, groove for the jugular vein; **jf**, jugular foramen; **ke**, median keel; **lr**, lateral recess; **mr**, medial recess; **occd**, occipital condyle; **opt?**¸optical foramen; **pc**, pars contacta; **pf**, perilymphatic foramen; **pocp**, paraoccipital process; **ppp**, posterior process of the parasphenoid; **prf**, prootic foramen; **pro**, prootic, **pt.at**, pterygoid attachment area; **tsob**, tectum supraorbitale.

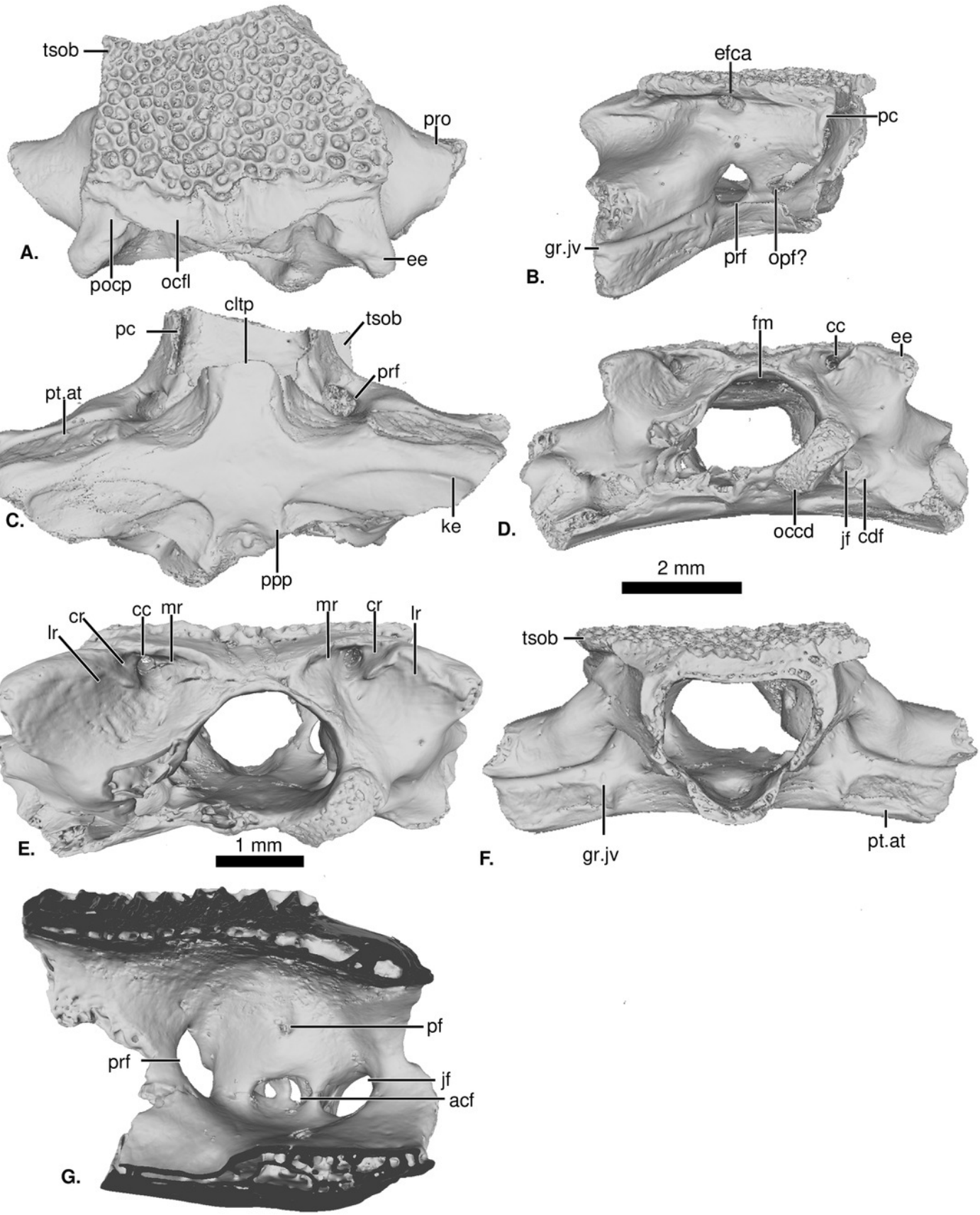
tsob
pro
A.
pocp
ocfl
ee
efca
pc
gr.jv
prf
opf?
B.
cltp
pc
tsob
prf
pt.at
C.
ke
ppp
fm
cc
ee
D.
occd
jf
cdf
2 mm
cr
cc
mr
mr
cr
lr
lr
E.
1 mm
tsob
F.
gr.jv
pt.at
pf
prf
jf
acf
G.

Figure 2

Internal morphology of the otic capsule of *Cretadhefdaa*

Inner ear in **A** anterior; **B** posterior; **C** dorsal; **D** ventral and **E** lateral views. **Abbreviations**: **aamp**, anterior ampulla; **accdt**, acoustic duct; **acl**, anterior canal; **eddt**, endolymphatic duct; **lamp**, lateral ampulla; **lch**, lateral chamber; **lcl**, lateral canal; **otch**, otic chamber; **ovw**, oval window; **pamp**, posterior ampulla; **pcl**, posterior canal; **psi**, posterior sinus; **pycist**, perilymphatic cistern; **pydt**, perilymphatic duct; **rwd**, round window; **sups**, superior sinus; **utr**, utricle.

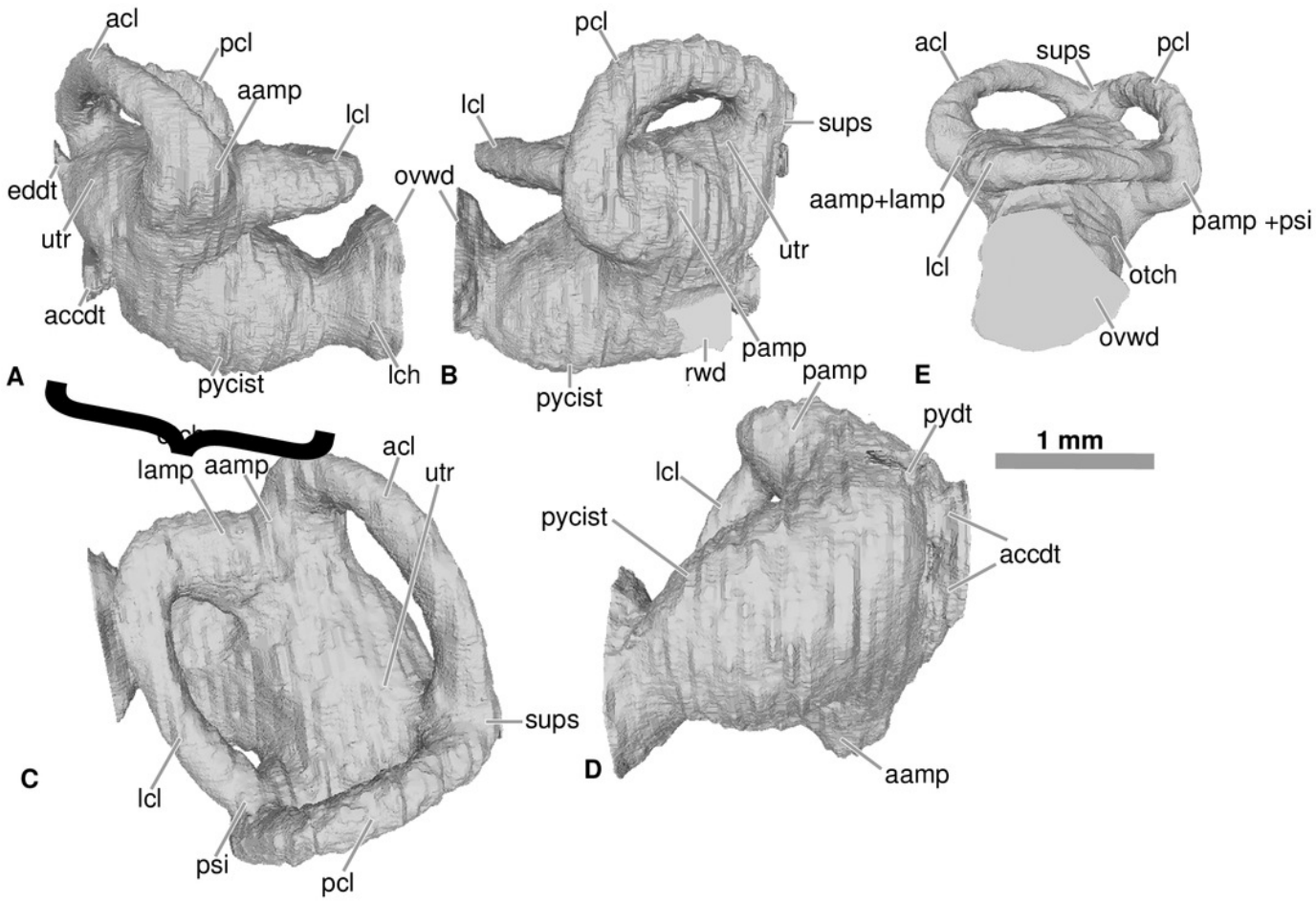

Figure 3

Cranial elements of *Cretadhefdaa*

A – E UCRC-PV95, incomplete squamosal in **A**, dorsal; **B** medial; **C** anterior; **D** posterior and **E** ventral views; **F–G** UCRC-PV94, incomplete maxilla in **F** lateral, **G** medial and **H** dorsomedial views. **Abbreviations**: **cd**, crista dentalis; **fps?**, frontoparietal suture ?; **lh**, lamina horizontalis; **mr**, medial ridge; **or**, ornamentation; **par?**; palatine articulation; **pzm**, processus zygomatico-maxillaris; **qjf?**; quadratojugal facet ?; **sqvl**, squamosal ventral lamina; **sqvr**, squamosal ventral ridge; **squvre**, squamosal ventral recess; **tm**, temporal margin.

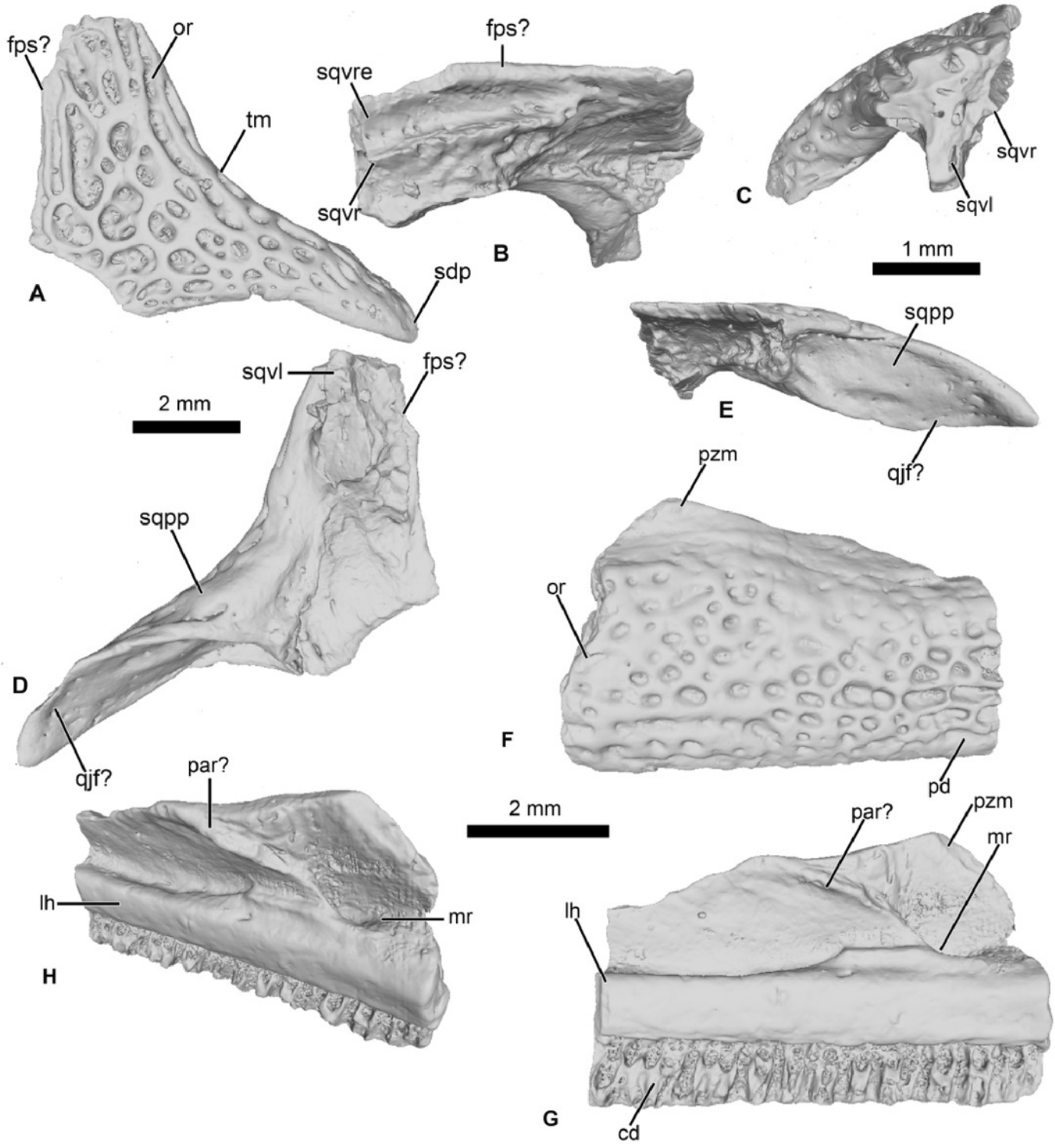
fps?
or
tm
sdp
A
fps?
sqvre
sqvr
B
sqvr
sqvl
C
1 mm
sqvl
fps?
2 mm
sqpp
D
qjf?
sqpp
E
qjf?
pzm
or
F
pd
2 mm
par?
lh
mr
H
par?
pzm
mr
lh
G
cd

Figure 4

Vertebral element of *Cretadhefdaa*

A–C UCRC-PV97, presacral centrum in **A** dorsal; **B** ventral and **C** right lateral views; **D**–**I** UCRC-PV98 incomplete possible presacral vertebra IV in **D** anterior; **E** posterior; **F** dorsal; **G** ventral; **H** left lateral and **I** right lateral views; **J–N** UCRC-PV101, incomplete possible presacral VIII in **J** anterior; **K** posterior; **L** dorsal; **M** ventral and **N** left lateral views; **O–R** UCRC-PV103, incomplete sacral vertebra in **O** anterior; **P** posterior; **Q** right lateral and **R** ventral views. **Abbreviations**: **act**, anterior cotyle; **nsp**, neural spine; **pcd**, posterior condyle; **poz**, postzygapophyse; **prz**, prezygapophyse; **psl**, posterior lamina; **spf**, spinal foramen; **stp**, sacral transverse process; **tp**, transverse process.

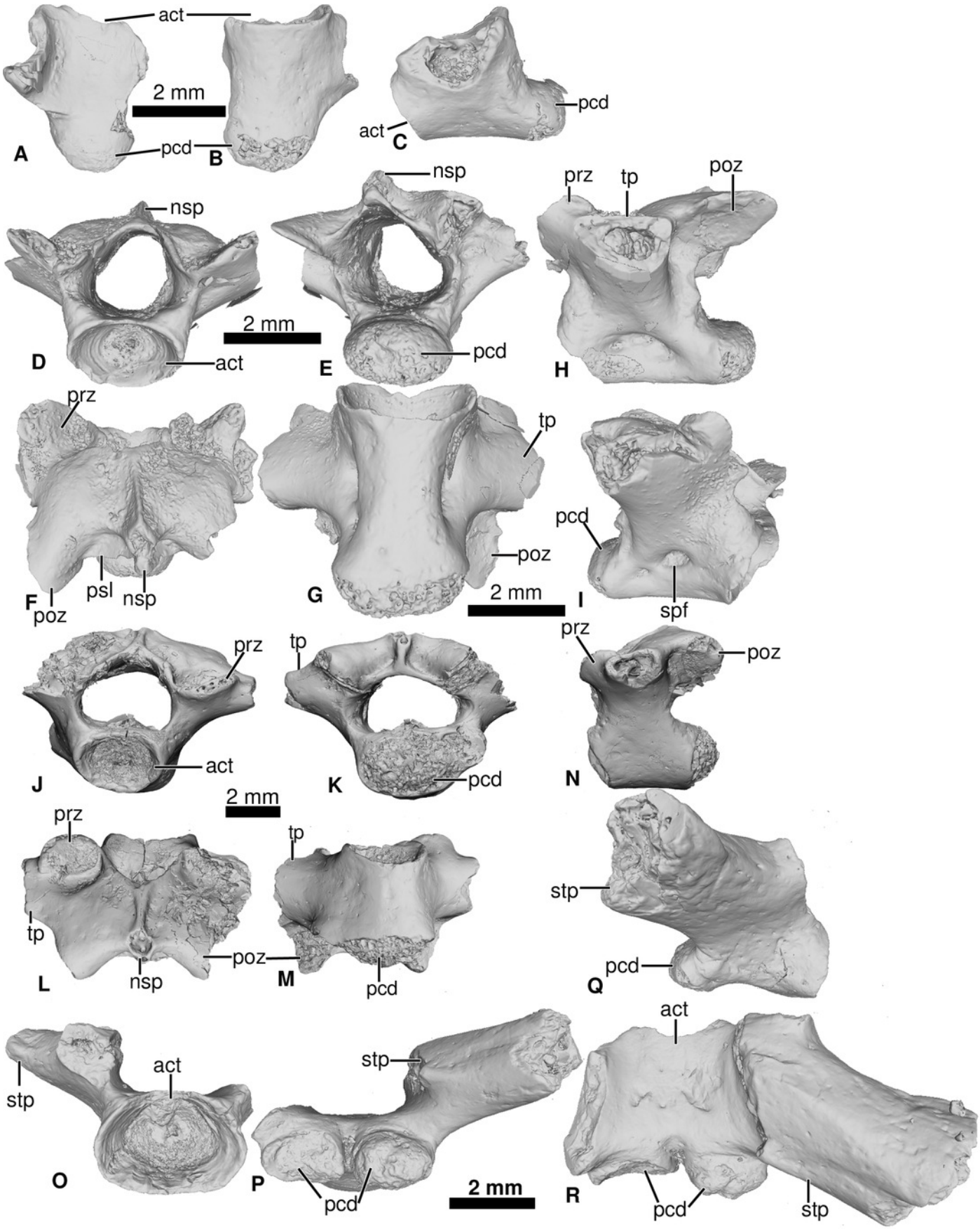
act
2 mm
pcd
A
B
act
pcd
C
nsp
nsp
2 mm
pcd
D
act
E
prz
tp
poz
H
prz
tp
pcd
poz
spf
I
F
poz
psl
nsp
G
2 mm
prz
poz
J
act
tp
K
pcd
N
2 mm
prz
tp
tp
poz
L
nsp
M
pcd
stp
pcd
Q
act
stp
O
stp
P
pcd
2 mm
act
R
pcd
stp

Figure 5

Comparison between the braincases of *Cretadhefdaa*, *Beelzebufo* and Ceratophryidae

A *Cretadhefdaa* in posterior view (UCRC-PV64); **B** *Beelzebufo* braincase in posterior view (taken from Evans et al., 2014: fig. 22C) and **C** braincase of *Ceratophrys aurita* in posterior view (CAS:Herp:84998; MorphoSource ARK: ark:/87602/m4/M16099). Black arrows point to the recesses discussed in the text

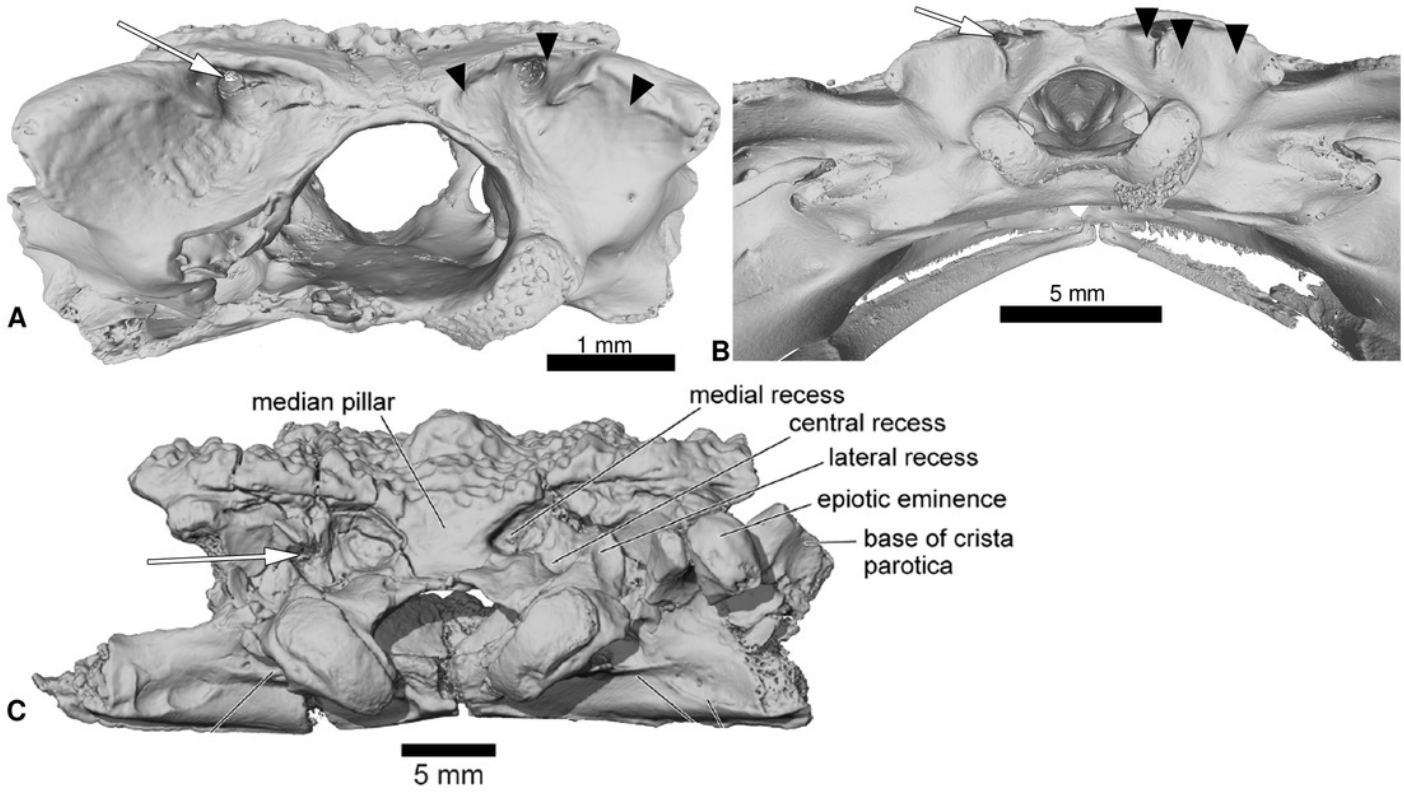

Figure 6

Neobatrachia? and indeterminate ilium from Kem Kem beds

A–C, UCRC-PV104, incomplete humerus in **A** ventral; **B** dorsal and **C** lateral views; **D–G**, UCRC-PV105, left ilium in **D** lateral; **E** medial; **F** posterior and **G** dorsal views . **Abbreviations**: **acf**, acetabular fossa; **acr**, acetabular rim; **dae**, dorsal acetabular expansion; **dc**, dorsal crest; **dpm**, dorsal prominence; **fc**, fossa cubitalis; **hb**, humeral ball; **ij**, ilioischiatic juncture; **ish**, iliac shaft; **lc**, lateral crest; **mob**, medial oblique ridge; **olsc**; olecranon scar; **pz**, preacetabular zone; **recd**, radial (lateral) epicondyle; **shft**, shaft; **uecd**, ulnare (medial) epicondyle; **vae**, ventral acetabular expansion; **vc**, ventral crest.

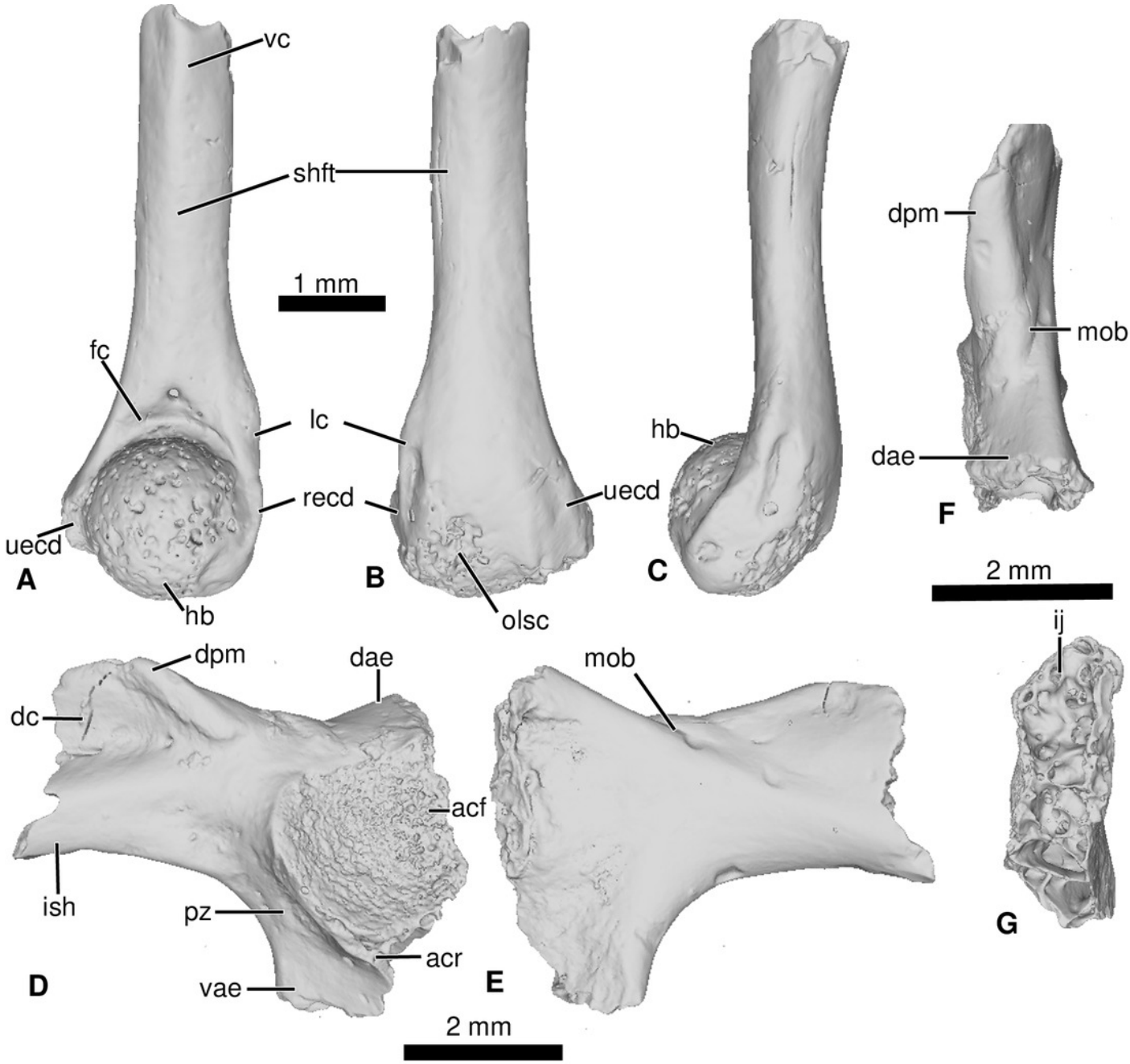
vc
shft
1 mm
fc
lc
recd
uecd
hb
A
B
olsc
C
hb
uecd
dpm
mob
dae
F
2 mm
ij
G
dpm
dae
dc
acf
ish
pz
acr
vae
D
mob
E
2 mm

Figure 7

Strict consensus of 60 MPTs of 1362 steps (CI = 0.139; RI = 0.418) from the analysis under EW

† represents extinct taxon, red circle represents Neobatrachia node (excluding *Heleophryne*), light blue circle represents Ceratophryidae node.

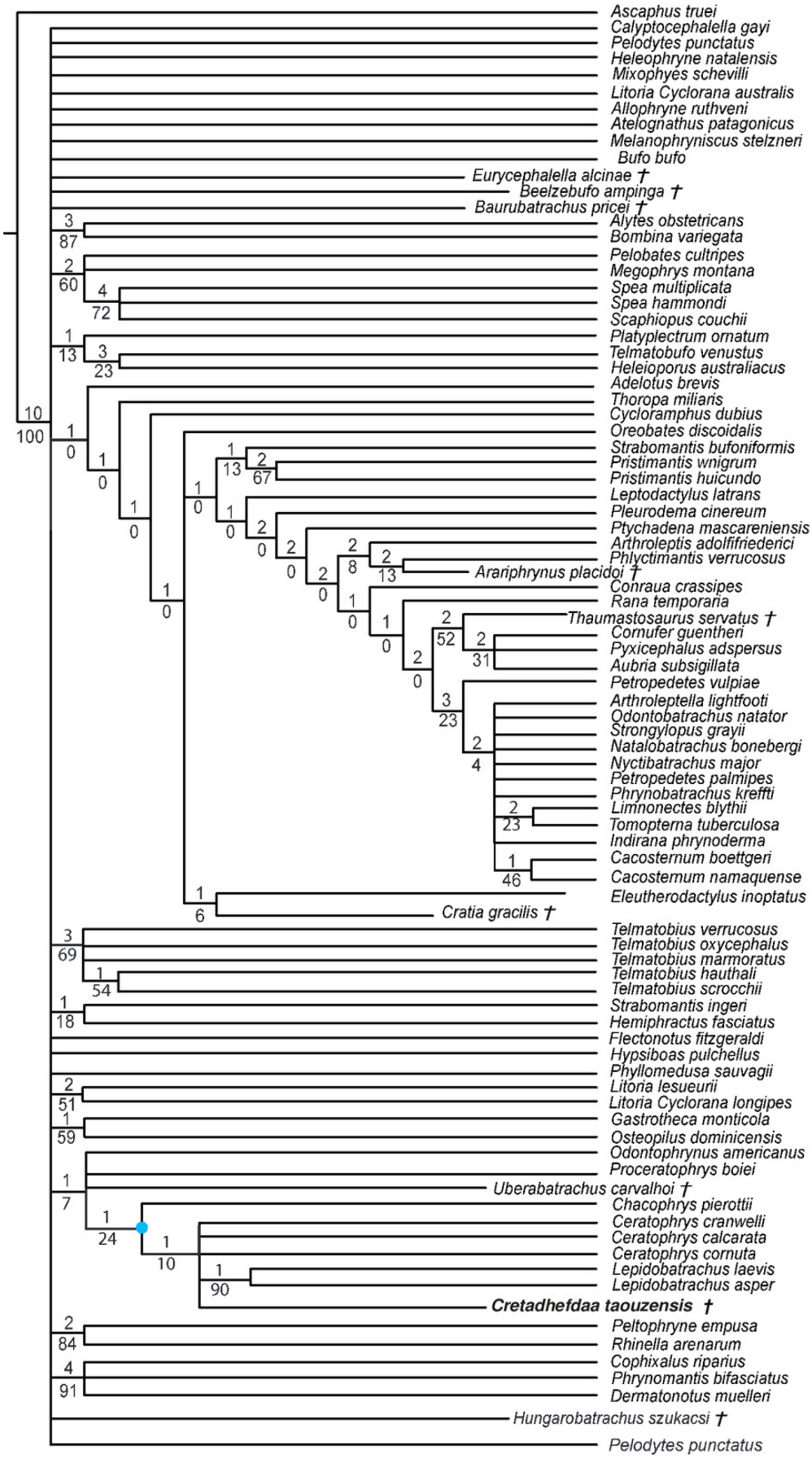
Ascaphus truei
Calyptocephalella gayi
Pelodytes punctatus
Heleophryne natalensis
Mixophyes schevilli
Litoria Cyclorana australis
Allophryne ruthveni
Atelognathus patagonicus
Melanophryniscus stelzneri
Bufo bufo
Eurycephalella alcinae †
Beelzebufo ampinga †
Baurubatrachus pricei †
Alytes obstetricans
Bombina variegata
Pelobates cultripes
Megophrys montana
Spea multiplicata
Spea hammondi
Scaphiopus couchii
Platyplectrum ornatum
Telmatobufo venustus
Heleioporus australiacus
Adelotus brevis
Thoropa miliaris
Cycloramphus dubius
Oreobates discoidalis
Strabomantis bufoniformis
Pristimantis wnigrum
Pristimantis huicundo
Leptodactylus latrans
Pleurodema cinereum
Ptychadena mascareniensis
Arthroleptis adolfifriederici
Phlyctimantis verrucosus
Arariphrynus placidoi †
Conraua crassipes
Rana temporaria
Thaumastosaurus servatus †
Cornufer guentheri
Pyxicephalus adspersus
Aubria subsigillata
Petropedetes vulpiae
Arthroleptella lightfooti
Odontobatrachus natator
Strongylopus grayii
Natalobatrachus bonebergi
Nyctibatrachus major
Petropedetes palmipes
Phrynobatrachus kreffti
Limnonectes blythii
Tomopterna tuberculosa
Indirana phrynoderma
Cacosternum boettgeri
Cacosternum namaquense
Eleutherodactylus inoptatus
Cratia gracilis †
Telmatobius verrucosus
Telmatobius oxycephalus
Telmatobius marmoratus
Telmatobius hauthali
Telmatobius scrocchii
Strabomantis ingeri
Hemiphractus fasciatus
Flectonotus fitzgeraldi
Hypsiboas pulchellus
Phyllomedusa sauvagii
Litoria lesueurii
Litoria Cyclorana longipes
Gastrotheca monticola
Osteopilus dominicensis
Odontophrynus americanus
Proceratophrys boiei
Uberabatrachus carvalhoi †
Chacophrys pierottii
Ceratophrys cranwelli
Ceratophrys calcarata
Ceratophrys cornuta
Lepidobatrachus laevis
Lepidobatrachus asper
Cretadhefdaa taouzensis †
Peltophryne empusa
Rhinella arenarum
Cophixalus riparius
Phrynomantis bifasciatus
Dermatonotus muelleri
Hungarobatrachus szukacsi †
Pelodytes punctatus

Figure 8

Strict consensus of 10 MPTs of 1355 steps (CI = 0.174; RI = 0.556) from the analysis under EW excluding *Arariphrynus placidoi*

† represents extinct taxon, red circle represents Neobatrachia node (excluding *Heleophryne*), and light blue circle represents Ceratophryidae node.

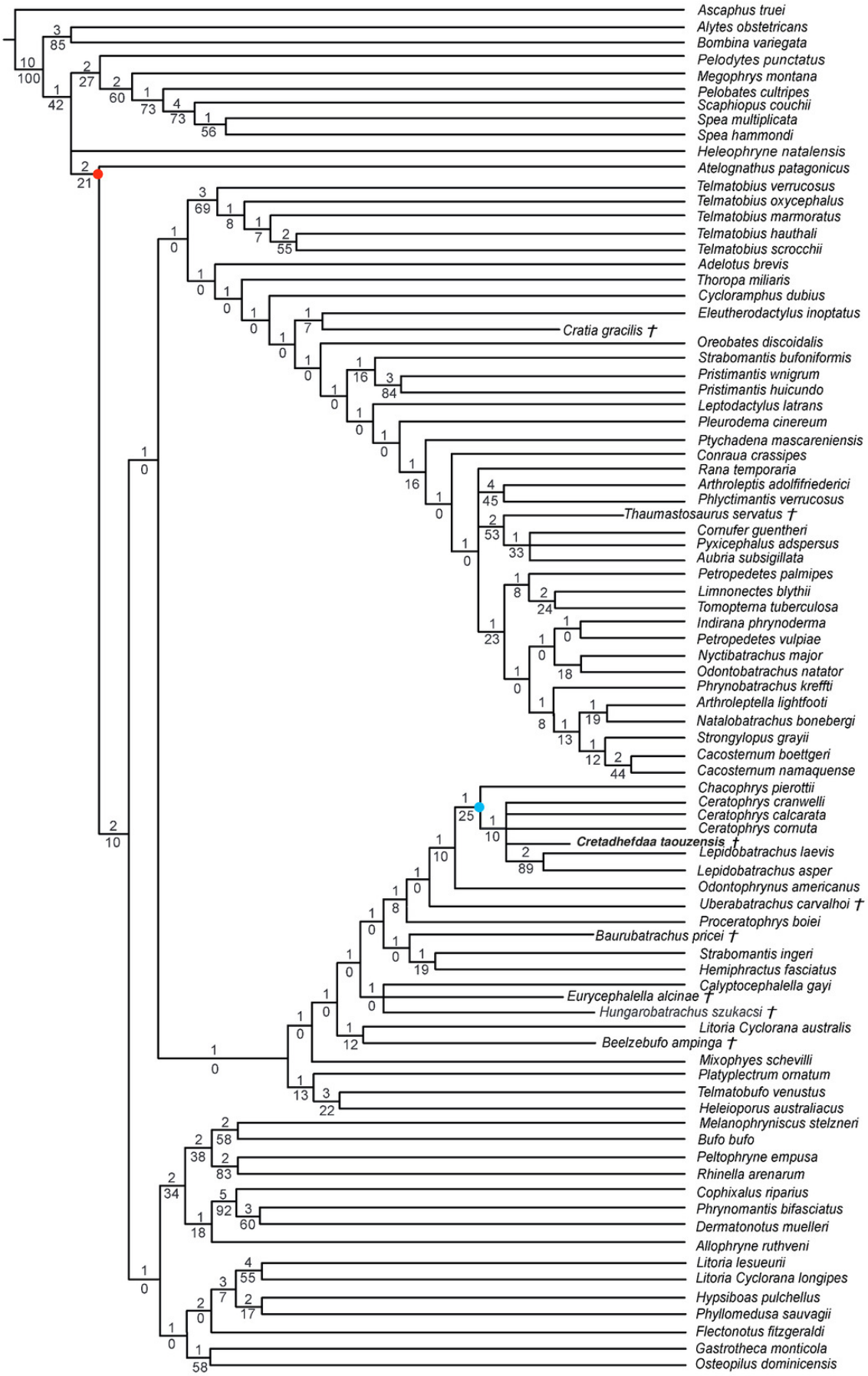
Ascaphus truei
Alytes obstetricans
Bombina variegata
Pelodytes punctatus
Megophrys montana
Pelobates cultripes
Scaphiopus couchii
Spea multiplicata
Spea hammondi
Heleophryne natalensis
Atelognathus patagonicus
Telmatobius verrucosus
Telmatobius oxycephalus
Telmatobius marmoratus
Telmatobius hauthali
Telmatobius scrocchii
Adelotus brevis
Thoropa miliaris
Cycloramphus dubius
Eleutherodactylus inoptatus
Cratia gracilis †
Oreobates discoidalis
Strabomantis bufoniformis
Pristimantis wnigrum
Pristimantis huicundo
Leptodactylus latrans
Pleurodema cinereum
Ptychadena mascareniensis
Conraua crassipes
Rana temporaria
Arthroleptis adolfifriederici
Phlyctimantis verrucosus
Thaumastosaurus servatus †
Cornufer guentheri
Pyxicephalus adspersus
Aubria subsigillata
Petropedetes palmipes
Limnonectes blythii
Tomopterna tuberculosa
Indirana phrynoderma
Petropedetes vulpiae
Nyctibatrachus major
Odontobatrachus natator
Phrynobatrachus kreffti
Arthroleptella lightfooti
Natalobatrachus bonebergi
Strongylopus grayii
Cacosternum boettgeri
Cacosternum namaquense
Chacophrys pierottii
Ceratophrys cranwelli
Ceratophrys calcarata
Ceratophrys cornuta
Cretadhefdaa taouzensis †
Lepidobatrachus laevis
Lepidobatrachus asper
Odontophrynus americanus
Uberabatrachus carvalhoi †
Proceratophrys boiei
Baurubatrachus pricei †
Strabomantis ingeri
Hemiphractus fasciatus
Calyptocephalella gayi
Eurycephalella alcinae †
Hungarobatrachus szukacsi †
Litoria Cyclorana australis
Beelzebufo ampinga †
Mixophyes schevilli
Platyplectrum ornatum
Telmatobufo venustus
Heleioporus australiacus
Melanophryniscus stelzneri
Bufo bufo
Peltophryne empusa
Rhinella arenarum
Cophixalus riparius
Phrynomantis bifasciatus
Dermatonotus muelleri
Allophryne ruthveni
Litoria lesueurii
Litoria Cyclorana longipes
Hypsiboas pulchellus
Phyllomedusa sauvagii
Flectonotus fitzgeraldi
Gastrotheca monticola
Osteopilus dominicensis

Figure 9

Strict consensus of 190 MPTs of 1395 steps (CI =0.126 ; RI = 0.247) from the analysis under EW, excluding *Arariphrynus placidoi* and using a constraint topology based on molecular phylogenetic analyses

† represents extinct taxon.

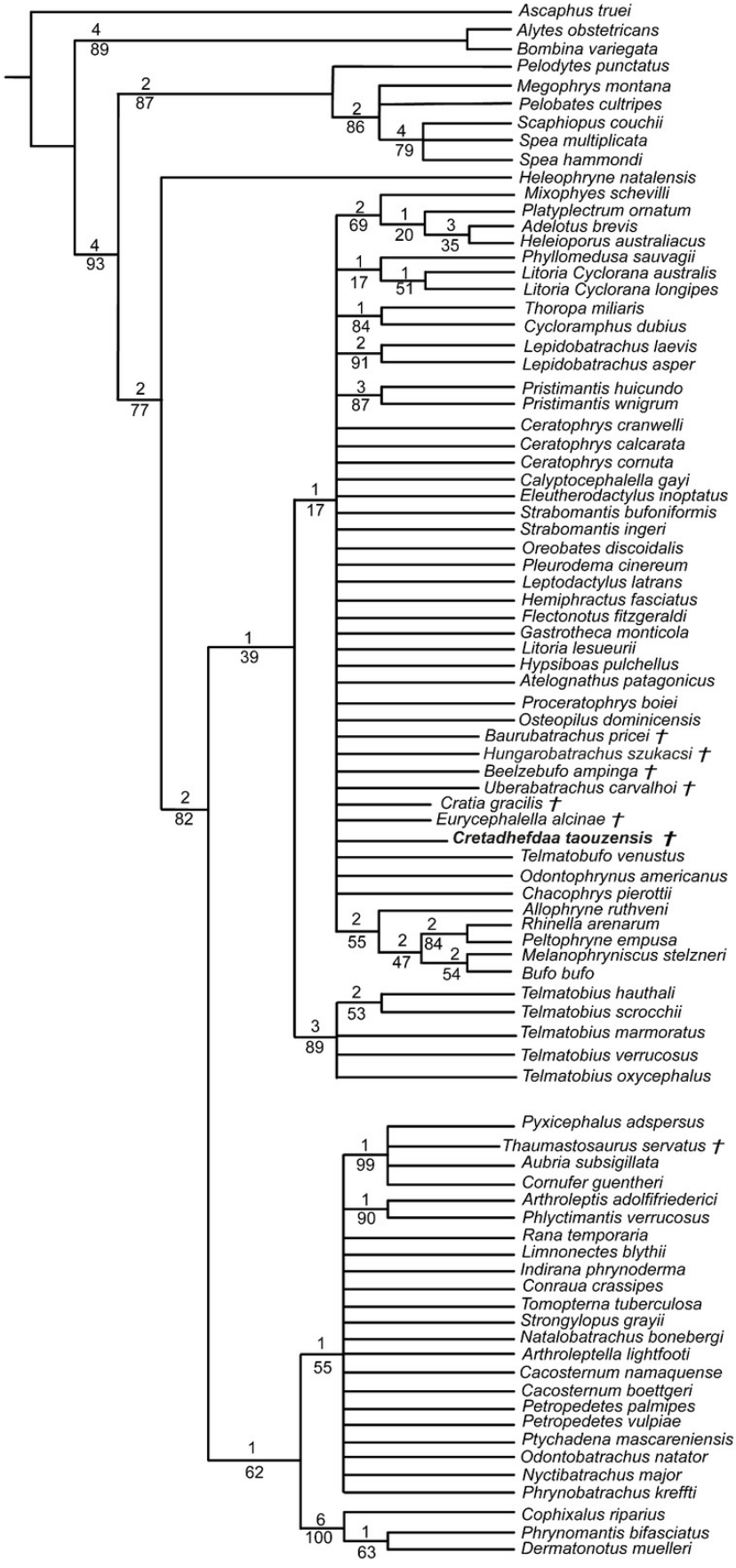
Ascaphus truei
Alytes obstetricans
Bombina variegata
Pelodytes punctatus
Megophrys montana
Pelobates cultripes
Scaphiopus couchii
Spea multiplicata
Spea hammondi
Heleophryne natalensis
Mixophyes schevilli
Platyplectrum ornatum
Adelotus brevis
Heleioporus australiacus
Phyllomedusa sauvagii
Litoria Cyclorana australis
Litoria Cyclorana longipes
Thoropa miliaris
Cycloramphus dubius
Lepidobatrachus laevis
Lepidobatrachus asper
Pristimantis huicundo
Pristimantis wnigrum
Ceratophrys cranwelli
Ceratophrys calcarata
Ceratophrys cornuta
Calyptocephalella gayi
Eleutherodactylus inoptatus
Strabomantis bufoniformis
Strabomantis ingeri
Oreobates discoidalis
Pleurodema cinereum
Leptodactylus latrans
Hemiphractus fasciatus
Flectonotus fitzgeraldi
Gastrotheca monticola
Litoria lesueurii
Hypsiboas pulchellus
Atelognathus patagonicus
Proceratophrys boiei
Osteopilus dominicensis
Baurubatrachus pricei †
Hungarobatrachus szukacsi †
Beelzebufo ampinga †
Uberabatrachus carvalhoi †
Cratia gracilis †
Eurycephalella alcinae †
Cretadhefdaa taouzensis †
Telmatobufo venustus
Odontophrynus americanus
Chacophrys pierottii
Allophryne ruthveni
Rhinella arenarum
Peltophryne empusa
Melanophryniscus stelzneri
Bufo bufo
Telmatobius hauthali
Telmatobius scrocchii
Telmatobius marmoratus
Telmatobius verrucosus
Telmatobius oxycephalus
Pyxicephalus adspersus
Thaumastosaurus servatus †
Aubria subsigillata
Cornufer guentheri
Arthroleptis adolfifriederici
Phlyctimantis verrucosus
Rana temporaria
Limnonectes blythii
Indirana phrynoderma
Conraua crassipes
Tomopterna tuberculosa
Strongylopus grayii
Natalobatrachus bonebergi
Arthroleptella lightfooti
Cacosternum namaquense
Cacosternum boettgeri
Petropedetes palmipes
Petropedetes vulpiae
Ptychadena mascareniensis
Odontobatrachus natator
Nyctibatrachus major
Phrynobatrachus kreffti
Cophixalus riparius
Phrynomantis bifasciatus
Dermatonotus muelleri